HIGH-EFFICIENCY CARBON DIOXIDE CAPTURE USING POROUS DOUBLE NETWORK GELS COATED WITH MICROALGAL AMINO ACID SALT SOLUTION

By

Annaliese Marks

A THESIS

Submitted to
Michigan State University
in partial fulfillment of the requirements
for the degree of

Biosystems Engineering – Master of Science

2024

ABSTRACT

Carbon dioxide emissions from industrial sources such as power plants pose a significant problem for environmental health. The goal of this research was to develop an absorbent material that is effective, efficient, and sustainable in capturing carbon dioxide gas. Absorption testing was conducted at CO_2 concentrations of 10%, 30%, and 50% by volume, using various amounts of microalgal amino acid salt solution (MAASS) embedded in porous gel. The increased surface area of the gel enhanced CO_2 absorption as larger volumes of MAASS were used, improving the absorption capacity compared to previous absorbent materials. Material analysis indicated that porous gel selectively absorbs amino acids from the MAASS, further increasing CO_2 absorption capacity compared to using liquid MAASS alone.

To optimize absorption conditions for flue gas from a power plant, the objectives were to maximize the absorption rate and equilibrium absorption volume while minimizing MAASS usage and CO_2 content in the absorption environment. Multi-objective optimization results indicated that CO_2 absorption from flue gas using 8-13 or 20-23 mL of MAASS in the porous gel achieved optimal absorption rate and absorption volume. Initial testing of a column-based system under these conditions demonstrated an absorption capacity of 2.24 mol CO_2/mol amine, which is a 75% higher capacity than using liquid MAASS alone. Further development of this system is needed to enable the design of industrial-scale absorption columns that can capture carbon emissions from sources such as power plants before they are released into the atmosphere.

ACKNOWLEDGEMENTS

First, I would like to thank MSU Climate Change Research Support Program for funding my research project. I would also like to thank Dr. Shengqiang Cai at UC San Diego for providing the porous double network gel. Without this support, my project would not have been possible.

Next, I would like to thank the multiple labs and analysis centers that assisted me in acquiring the data I needed for my research. This includes the University of Georgia for providing carbohydrate analysis, MSU Mass Spectrometry and Metabolomics Core for providing LCMS amino acid analysis, MSU Center for Advanced Microscopy for helping execute SEM and EDX imaging, and MSU ADREC for their research support.

I would also like to thank my thesis committee, Dr. Wei Liao, Dr. Yan (Susie) Liu, and Dr. Chris Saffron for their mentorship and guidance.

To Dr. Wei Liao and Dr. Sibel Uludag-Demirer, I am so grateful for your mentorship, flexibility, compassion, and leadership during the 6 ½ years I have spent in the Liao lab group.

Thank you also to my many lab mates I have had the pleasure of working with throughout my time at MSU, and to all the students and faculty in MSU Biosystems Engineering who have been such great friends and mentors to me.

Finally, thank you to my friends and family, especially my twin sister Juliana Marks, without whom I wouldn't be here.

TABLE OF CONTENTS

LIST OF TABLES

LIST OF FIGURES

LIST OF ABBREVIATIONS

AASS	Amino acid salt solution
CO_2	Carbon dioxide
EDX	Energy-dispersive X-ray spectroscopy
GC-MS	Gas chromatography – mass spectrometry
LCA	Life cycle analysis
LCMS	Liquid chromatography–mass spectrometry
MAASS	Microalgal amino acid salt solution
MBAA	N,N'-Methylene bis(acrylamide)
MEA	Monoethanolamine
MOOA	Multi-objective optimization analysis
NSGA	Non-dominated Sorting Genetic Algorithm
SEM	Scanning electron microscopy
TEMED	N,N,N',N'-tetramethyl-ethylenediamine

CHAPTER 1: LITERATURE REVIEW

1.1 INTRODUCTION

This chapter introduces previous research on the use of carbon dioxide absorbents and explores the possible use of porous double network gel in absorption technologies. It provides context for this research project, which examines the efficacy of porous double network gel as a combined absorption technology with microalgal amino acid salt solution.

The immense output of carbon dioxide in emissions from industrial and residential sectors is a well-known environmental problem. Flue gas from power plants and other industrial locations constitutes a major contributor to these emissions (EPA, 2024). Carbon dioxide significantly drives global warming because of its large-scale release and long atmospheric persistence (Tucker, 1995). This persistence exacerbates irreversible and harmful environmental changes, including global warming, irregular precipitation, and rising sea levels (Solomon et al., 2009). Therefore, reducing carbon emissions and/or mitigating carbon dioxide levels in the atmosphere is urgently needed to prevent catastrophic environmental impacts.

1.2 BACKGROUND

1.2.1 Carbon dioxide absorption processes

Absorption is a post-combustion method for capturing carbon dioxide. This method uses a liquid solvent, also called an absorbent, to capture carbon dioxide gas. The process relies on chemical reactions between the absorbent and CO_2 which enable the gas to be bound and absorbed into the solution. The production of a bare amine group is facilitated by an alkaline substance in the absorbent solution creating a basic pH level. These bare amine groups then react with the carbon dioxide to form new compounds of carbamates and bicarbonates, binding the

CO_2 within the absorbent solution. These absorption steps are illustrated in Figure 1. Subsequent desorption by heating causes the CO_2 to be released through the reverse of the chemical absorption process and potentially collected as pure CO_2. These absorption and desorption processes have the potential to be repeated in a cyclic capacity for reuse of the absorbent material.

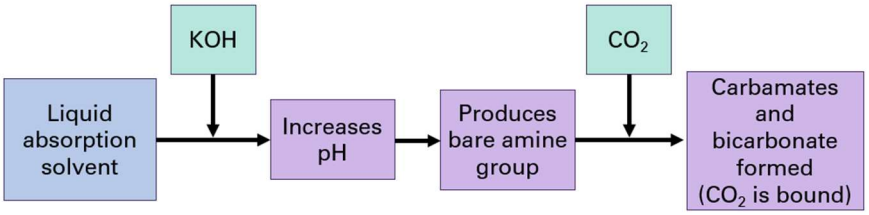

Figure 1. Carbon dioxide absorption reaction.

In the past, synthetic amines, particularly monoethanolamine (MEA), have been a common choice of solvent for carbon dioxide absorption processes. MEA is an amine solution that is produced by ammonolysis through a reaction between ammonia and ethylene oxide. The reaction is exothermic and requires high pressure and temperature, as well as subsequent distillation (Luis, 2016). The manufacturing process is similar for other commonly used solvents diethanolamine (DEA) and triethanolamine (TEA). The popularity of MEA as a solvent is due to its high CO_2 absorption capacity, particularly for the typical concentrations of CO_2 found in flue gas (Uludag-Demirer et al., 2023). However, the absorption potential of this solvent is not very efficient, reaching an absorption of only 0.368 mol CO_2/mol amine at a 1M MEA concentration (Aronu et al., 2011). Another large drawback of MEA is that it has an energy-intensive production process (Luis, 2016). This means that the material is not very environmentally friendly as an absorbent material due to the large energy usage needed in regeneration for reuse.

1.2.2 Amino acid salt solutions

Amino acid salt solutions have been found to be an ideal alternative solvent for carbon dioxide capture (Zhang et al., 2018). This is because they have high CO_2 absorption capacity while also having low degradation and evaporation during the absorption/desorption process. Amino acids commonly used for CO_2 absorption include glycine, proline, lysine, alanine, arginine, and sarcosine (Zhang et al., 2018). These solutions are prepared by dissolving the selected mixture of amino acids in deionized (DI) water and mixing them with an alkaline substance (Zhang et al., 2018), such as potassium hydroxide. Sodium and lithium are also common alkaline substances used in forming amino acid salt solutions. The absorbent solution is synthesized at a 1:1 molar ratio of amino acids to alkaline substance.

The absorption and desorption reactions of amino acid carbon capture are described in Figure 2. When a high-pH solution is first exposed to carbon dioxide, the deprotonated amine group reacts with CO_2 to form carbamate. The carbamate exists in equilibrium with bicarbonate and carbonate, with the equilibrium favoring bicarbonate formation. Subsequently, with elevated temperature, the carbamate hydrolyzes, producing bicarbonate and regenerating the amine group in its deprotonated form, allowing it to react with CO_2 again. This process can continue as long as hydrolysis occurs and the solution's pH supports the presence of deprotonated amine groups. Over time, further absorption reduces the solution's pH as bicarbonate and carbonate contribute to acidification. Ultimately, equilibrium is reached, with bicarbonate being the dominant product.

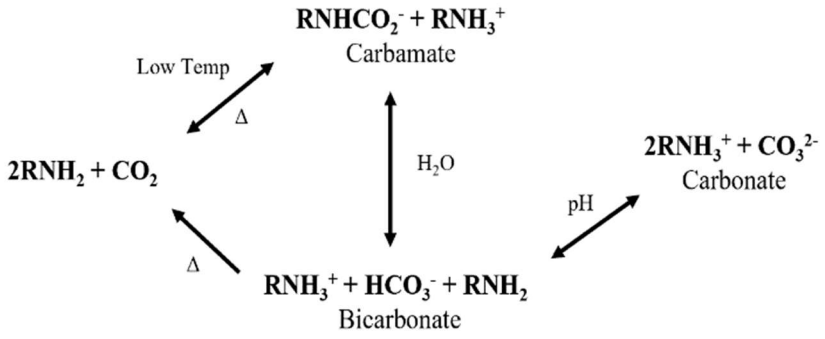

Figure 2. Amino acid carbon capture reaction process.

Research has been done to determine the amino acid and/or combination of amino acids with the greatest CO_2 absorption potential. The cycling potential of these combinations has also been explored by measuring the degradation of the amino acid salt solutions over several absorption/desorption cycles. Results show that lysine mixed with potassium hydroxide is the single amino acid with the highest CO_2 absorption capacity (Uludag-Demirer et al., 2023; Zhang et al., 2018). In addition, combining amino acids within the absorbent creates a higher CO_2 absorption capacity. The absorption capacity of the combined solution is greater than the expected capacity when summing the absorption capacity of the individual amino acids present in the solution (Uludag-Demirer et al., 2023; Zhang et al., 2018). However, this solution could be more efficient, since its absorption is usually around 0.6 mol CO_2/mol amine, which is not much higher than the capacity of the MEA absorbent.

For amino acid salt solutions to be used effectively in a cyclic capacity, they must have a low rate of degradation. This means that after multiple CO_2 absorption/desorption cycles, the solution will have a CO_2 absorption capacity comparable to its initial capacity. Degradation of the absorbent is caused by thermal instability or reaction with oxygen and other impurities in the input gas mixture (Azzi & White, 2016). Studies show that a greater distance between the amino

group and the carboxyl group in the AASS results in higher cyclic capacity (Ramezani et al., 2022; Song et al., 2012). Bulkier amino acid functional groups also contribute to higher cyclic capacity.

1.2.3 Microalgal amino acid salt solutions (MAASS)

Biological materials are also effective at capturing carbon dioxide (Zahed et al., 2021). Algae in particular have high CO_2 capture efficiency (Moreira & Pires, 2016). Algae use carbon as their main energy source for growth and require other nutrients such as ammonia, nitrogen, and phosphate (Moreira & Pires, 2016). Their high rate of growth and high photosynthetic efficiency contribute to their effectiveness at CO_2 capture (Song et al., 2019).

An abundance of research has been done on the use of flue gas from power plants as the carbon source for algae growth. For example, Cheah et al. compared the CO_2 fixation rate and biomass yield of different algae strains, along with different algal cultivation systems (Cheah et al., 2015). Pavlik et al. and Cutshaw et al. investigated the use of a pilot-scale photobioreactor for long-term algal cultivation. They found that using flue gas as the carbon source for the algae was successful in terms of feasibility, long-term stability, biomass productivity, and economics (Cutshaw et al., 2020; Pavlik et al., 2017). Moreira & Pires discuss how removing CO_2 from the atmosphere, particularly by using algae and seaweed, can help to mitigate negative environmental impacts. Their study also highlights algae biomass applications and algal biofuels, proving the positive environmental and economic impacts of algal carbon capture technologies (Moreira & Pires, 2016).

A review of algal CO_2 capture by Song et al. states that capturing CO_2 post-combustion is the most developed strategy for CO_2 capture. In addition, algae are a more energy-efficient technology for CO_2 capture compared to chemical absorbents. However, changes in culture pH,

changes in culture salinity, or impurities in the flue gas source may be detrimental to algal health (Song et al., 2019). Overall, these algal cultures that utilize flue gas are designed to be co-located at power plants and other flue gas sources. The specific location would depend on the culture technology being used but would likely be a small room inside the facility when using photobioreactors. Initial testing is often executed on a smaller lab scale using compressed gas as a source of CO_2.

Although there is a lot of existing research on the applications of algal cultivation in CO_2 capture, there is little research done so far on the capability of algal amino acid salt solutions in the absorption/desorption process. However, initial research suggests that the use of algae in absorbents increases the CO_2 capture potential. For example, Song et al. proposed a hybrid absorption/algae system (Song et al., 2019). This hybrid system would combine the use of an absorption solvent with algae cultivation, either in separate connected containers or in an integrated system. They predict that the synergy between the algae and absorbent will result in decreased regeneration energy and increased CO_2 absorption efficiency (Song et al., 2019). Beyond its ability to use CO_2 in flue gas as a carbon source for growth, existing algae biomass also has strong potential as a carbon dioxide absorbent.

Taking the absorbent/algae hybrid system further presents the possibility of an absorbent solution containing algae. Algae strains that are high in protein content also have a large quantity of amino acids. Therefore, these strains would be the most effective for use in a CO_2 absorbent. Through hydrolysis, the algae can be made into an algal amino acid salt solution for use as a CO_2 absorbent material (Smerigan et al., 2023). The method of preparing the algae biomass involves thermochemical treatment, centrifugation, acidification, and desorption before it is ready for use as an absorbent (Smerigan et al., 2023).

When compared with synthetic solvent solutions, MAASS has a significantly higher CO_2 absorption capacity (Smerigan et al., 2023). A synthetic solution containing glycine, alanine, proline, and lysine was compared to the MAASS. The findings of this study show that the CO_2 absorption capacity for MAASS is 1.27 mol CO_2/mol amine, which is triple the capacity of the synthetic AASS (Smerigan et al., 2023). These findings imply that other molecular components present in algae also contribute to absorption capacity, leading to an increased CO_2 absorption potential. This high absorption efficiency is ideal for optimizing CO_2 absorption.

In addition, the MAASS can later be recycled for use in biofuel applications. Algae are considered a third-generation biofuel since it is a marine biomass and is not produced from food crops (Alaswad et al., 2015). Biodiesel made from algae has been found to be an effective and environmentally friendly alternative to standard diesel (Baldev et al., 2018). This process involves transesterification of lipids present in the algae. For algae strains high in carbohydrates, bioethanol production is another possible biofuel application. This involves pretreatment and a subsequent fermentation process to prepare the algae bioethanol (Harun et al., 2014). There are multiple possible methods for these steps depending on what would be most effective for the strain of algae being used.

One of the challenges with the use of MAASS for CO_2 absorption is that the liquid algae solution is prone to excessive foaming during the absorption/desorption process. This foaming inhibits the effectiveness of the MAASS as a CO_2 absorbent. In addition, the absorption system will eventually need to be scaled up for broader use. These reasons, among others, present the need for an improved reactor design.

1.2.4 Hydrogels

The incorporation of gel technology may be beneficial in manufacturing a more effective reactor design. Hydrogels are commonly defined as "a water-swollen, and cross-linked polymeric network produced by the simple reaction of one or more monomers" (Ahmed, 2015). They are prepared using a monomer, an initiator, and a cross-linker to induce the chemical reactions needed to form the gel material (Ahmed, 2015). Hydrophilic gels are also often referred to as hydrogels, but they are distinct because of their ability to dissolve in water, which makes them more difficult to handle. Therefore, this study will focus on non-hydrophilic hydrogels.

Gel type can be classified based on physical structure, chemical composition, cross-linking type, or electrical charge (Ahmed, 2015). In addition, there are both natural and synthetic hydrogels. Natural hydrogels are formed using proteins and polysaccharides, while synthetic hydrogels use chemical methods to form the gel (Ahmed, 2015). Natural polymers are usually non-toxic and biodegradable. Cross-linking in hydrogels is what prevents them from dissolving in water. There are multiple methods for creating this type of structure in the material, including using a chemical reaction, ionizing radiation, or physical interactions (Ahmed, 2015).

1.2.5 Hydrogel applications

This gel technology is utilized for a wide range of applications, including robotics, the environment, and various biomedical and personal care uses (Saul & Williams, 2011; Sun et al., 2017). For example, one biomedical use of hydrogel involves arranging hydrogel pieces at spaced intervals around a spinal cord injury to allow neurons and astrocytes to attach and begin growth (Krsko et al., 2009). Another biomedical example is the use of hydrogel in tissue engineering. One study used the natural chemical compound genipin as a crosslinker with hydrogel to form engineered cartilage tissue (Zhang et al., 2011). Hydrogels are also widely used

in the application of controlled release systems, particularly drug delivery. Park et al. demonstrates the effectiveness of using hydrogel and polyelectrolyte complex for a sustained release of human growth hormone in a patient's body. The polyelectrolyte complex was used to create the slow release of the drug, and the hydrogel used was biodegradable for patient safety (Park et al., 2010).

One example of hydrogel usage in the environment is removing pollutants in wastewater treatment. Van Tran et al. investigated the use of three different shapes of hydrogels: beads, films, and nanocomposites. For each shape, they tested the effectiveness of the adsorption of heavy-metal ions, harmful dyes, radioactive waste, and other contaminants (Van Tran et al., 2018). Results indicated that the beads and nanocomposites were all-around very effective adsorbents, with all shapes highly successful at removing at least some specific elements. They also found that the hydrogel maintained comparable adsorption capacity for 10 adsorption/desorption cycles (Van Tran et al., 2018). In agriculture, hydrogel can be used to improve fertilizer and irrigation applications. Using a combined system of hydrogel and slow-release fertilizer can help with more efficient fertilizer application and reduction of irrigation frequency by improving water retention (Liu et al., 2022). In addition, Ying & Liu discussed some of the applications of hydrogels in robotics, such as wearable electronics. Skin-like hydrogels can be used as biosensors to monitor conditions such as pressure, temperature, humidity, pH, or glucose levels (Ying & Liu, 2021). However, there are some limitations based on sensitivity and response rate.

1.2.6 Porous double network gels

The gel type selected for this study is a porous double network gel. The materials used to create the gel were alginate, acrylamide, N,N'-Methylene bis(acrylamide) (MBAA), ammonium

persulfate, N,N,N',N'-tetramethyl-ethylenediamine (TEMED), and calcium sulfate dihydrate (Sun et al., 2017). MBAA is used as a crosslinker, which forms a bond to link two polymer chains. Ammonium persulfate is used as a thermal initiator that uses heat to generate free radicals, which initiate the polymerization reaction. TEMED is used as an accelerator, and calcium sulfate dihydrate is used as the ionic crosslinker. An ionic crosslinker forms an ionic bond between two oppositely charged polymer chains.

These porous double network gels were manufactured by first dissolving alginate (a polysaccharide) and acrylamide in deionized water. The MBAA and ammonium persulfate are mixed with the dissolved alginate and acrylamide to create a homogeneous mixture (Sun et al., 2017). This mixture is degassed and mixed with a combination of TEMED and calcium sulfate dehydrate. This new mixture is quickly poured into a mold and baked in an oven at 53 Celsius for 100 minutes to form the double network hydrogel (Sun et al., 2017). To create macropores or micropores in the gel, the double network hydrogel is frozen and subsequently freeze-dried. For a nonporous gel, the double network hydrogel is dried at room temperature after baking (Sun et al., 2017).

When porous gels are compared with nonporous gels, their mechanical properties (stiffness, strength, and stretchability) are similar. However, porous gels are able to absorb more liquid and can absorb it more quickly (Sun et al., 2017). Therefore, porous gels are more suitable for the application of CO_2 absorption by soaking the gel in the MAASS.

Most hydrogels are not very stretchable and are brittle, causing breakage when stretched to about 1.2 times the original length (Sun et al., 2012). However, the use of crosslinkers in hydrogel production improves stretchability and strength. Porous double network gels have two separate crosslinked chain networks, one with short chains and the other with long chains, adding

even more toughness to the gel. This results in an increased stretching capacity of around 20 times the original length (Sun et al., 2012). Experimentation showed the porous double network gels to be relatively tough, allowing improved mechanical properties such as toughness and stretchability. However, increased swelling due to greater solution uptake will result in poorer mechanical properties (Sun et al., 2017).

Good mechanical strength is also important for the recyclability of hydrogels (Van Tran et al., 2018). However, the absorption capacity of porous double network gels in a second round of absorption is less than the initial capacity, even after being fully dried (Sun et al., 2017). Therefore, it may be more effective to use hydrogels in combination with MAASS as a single-use system. Alternatively, modifications could be made to allow the gel to be recycled without soaking it in the MAASS a second time.

1.3 KNOWLEDGE GAPS

When comparing MEA, AASS, and MAASS as carbon dioxide absorbents, MAASS is the most efficient. In addition, this material is environmentally friendly in terms of its ability to be regenerated and reused. These characteristics make MAASS the best option to pursue for absorption optimization. However, this material lacks the effectiveness of the other options due to the structural issues caused by the foaming of the algae solution. As discussed previously, there is also little research thus far on the use of MAASS for absorption of CO_2. The characteristics of MAASS need to be investigated to better understand their effectiveness as a carbon dioxide absorbent. This should include composition analysis, mass spectrometry, and nuclear magnetic resonance. In addition, there is a need for an improved absorption/desorption reactor design that can be scaled up for future industrial use. When using MAASS, the properties of algae need to be considered for optimal reactor design.

With the abundance of existing applications using gel technology, its application with MAASS in the CO_2 absorption/desorption process could be beneficial. Benefits of incorporating this technology could include additional structural support or improved scalability. However, there is not yet any existing research on the feasibility of this idea. Therefore, this study will analyze the characteristics of porous double network gels when soaked in MAASS. This will include studying effects of the porosity and surface area of the gel on the uptake of the MAASS and the effectiveness of CO_2 absorption. In designing this study, a new reactor setup will be manufactured and tested to investigate the efficacy of the gel for use in CO_2 absorption. Gel pieces soaked in MAASS will be sealed in a reactor to test CO_2 absorption effectiveness and capacity. A mass and energy balance and life cycle analysis will also be performed to evaluate the environmental impact and energy requirements of the proposed system. The goal, hypothesis, and objectives of this study are listed below:

1.4 RESEARCH GOAL AND OBJECTIVES

The goal is to develop an effective, efficient, and environmentally friendly CO_2 capture technology for the power industry.

The research objectives include:

1. Analyzing the characteristics of the MAASS.
2. Designing a bench-scale absorption reactor to study the CO_2 absorption of MAASS held in porous double network gels.
3. Measuring absorption capacity of porous double network gels containing different volumes of MAASS.
4. Performing multi-objective optimization to determine the most efficient porous gel +

MAASS combination.

5. Conducting an LCA for CO_2 absorption using MAASS held in porous double network gel.

1.5 RESEARCH HYPOTHESIS

The hypothesis is that combining microalgal amino acid salt solution (MAASS) and porous double network gel could create a new, bio-based CO_2 absorbent that significantly enhances CO_2 capture efficiency compared to existing CO_2 capture technologies. Specifically, the incorporation of porous gel is expected to improve structural stability and boost the CO_2 absorption capacity of MAASS. This is based on the premise that the CO_2 absorption capacity of MAASS is strongly influenced by the exposed surface area of the absorbent material.

CHAPTER 2: MATERIAL ANALYSIS OF MICROALGAL AMINO ACID SALT SOLUTION AND POROUS GEL

2.1 INTRODUCTION

Previous research has proven the high efficiency of microalgal amino acid salt solution (MAASS) as a CO_2 capture technology (Smerigan et al., 2023). However, the material qualities of MAASS and the reasoning for this high efficiency are not fully understood. This chapter discusses the preparation methods for MAASS and porous gel and delves deeper into the material components of MAASS. The use of porous gel as a medium to hold MAASS during absorption has also not yet been tested. Therefore, the dynamics of MAASS uptake into the porous gel are explored using kinetics and SEM imaging.

2.2 MATERIALS AND METHODS

2.2.1 Microalgal amino acid salt solution preparation

The most important materials used within this study are the microalgal amino acid salt solution (MAASS) and the porous double network gel. The MAASS is prepared by first processing solid algae biomass (species *Chlorella sorokiniana*) mixed with potassium hydroxide (KOH) through a thermochemical treatment process using a 2L Parr reactor (Smerigan et al., 2023). This process lyses the algae cells to release the amino acids present in the algae, maximizing the free amino acids in the algal solution, to form the algal amino acid salt solution. A centrifugation step (using an Allegra X-12R Centrifuge at 5°C and 10,000 rpm for 10 min) then filters out the algae solids for usage of the remaining liquid solution. Next, an acidification step purges the algal solution with carbon dioxide to neutralize it. A final desorption step is used to deprotonate the amino acids and prepare the solution for carbon dioxide absorption.

The KOH present within MAASS was previously determined to not affect CO_2 absorption capacity (Smerigan et al., 2023). According to the previously calculated mass balance on the flow of KOH during MAASS preparation, over 90% of KOH mass is eliminated through chemical reactions in the Parr reactor, the solid pellet post-centrifugation, and the post-acidification solids. The remaining potassium content is inactivated during acidification and is present as potassium bicarbonate (Smerigan et al., 2023).

2.2.2 Porous double network gel preparation

The porous double network gel used in this study was provided by Dr. Shengqiang Cai at UC San Diego. As discussed in section 1.2.6, the materials used in forming this gel include alginate, acrylamide (AAm) (99+%), N,N'-Methylene bis(acrylamide) (MBAA), ammonium persulfate (APS) (>98%), N,N,N',N'-tetramethyl-ethylenediamine (TEMED) (>99%), and calcium sulfate dihydrate (98%) (Sun et al., 2017). The manufacturing of porous double network gel follows the process detailed by Sun et al., and involves mixing, degassing, sonication, baking within a mold, freezing, and drying (Sun et al., 2017). The shrunken/collapsed quality of the initially dry porous gel pieces is caused by the polymer chains being pulled together during drying by the surface tension in the water (Ahmed, 2015).

2.2.3 Absorbent material preparation

Once the MAASS and porous gels are prepared, the absorbent material can be assembled. Each porous gel piece is weighed, and its length and diameter are measured in centimeters. The gel pieces are then soaked in 50 mL glass beakers containing about 40 mL of MAASS each until the desired volume of about 4 mL is absorbed (about 3 hours). This soaking volume of MAASS was chosen so that the gel pieces would be fully submerged while soaking. After soaking, the gel pieces are removed and held above the container until they stop dripping. Then the pieces are

weighed, and the length and diameter are measured again. These values are compared to the initial measurements to calculate how much the gel has swollen in size and to calculate the weight of MAASS that it has absorbed. The density of MAASS is about 1 g/mL, so a gain of 1 g in gel weight would equal an absorbed volume of 1 mL of MAASS. An illustration of this soaking process is given in Figure 3.

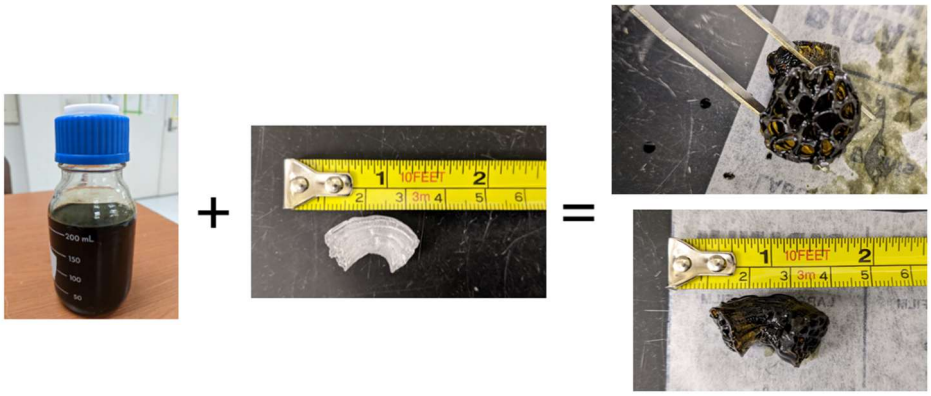

Figure 3. Porous gel + MAASS absorbent preparation process.

2.2.4 Material analysis

Carbohydrate analysis was performed externally by the University of Georgia Complex Carbohydrate Research Center. Glycosyl composition analysis was executed using gas chromatography – mass spectrometry (GC-MS). After neutralization and purification of the MAASS, molecular weight determination was performed using size-exclusion chromatography (SEC). Proton nuclear magnetic resonance (H-NMR) was also performed on the fractions from the 3 glycosyl composition analysis peaks.

Amino acid analysis was done through the Michigan State University Mass Spectrometry and Metabolomics Core. Samples were prepared at a 1000x dilution due to the high concentration of protein in the MAASS. LCMS was performed using a Waters Xevo TQS Micro.

Each sample vial analyzed contained the diluted sample, internal standards, external standards, and Milli-Q ultrapure water. Raw results from instrument calibration were reported in uM and the final amino acid concentration results were reported in mM after adjustment for dilution.

SEM and EDX imaging was done through the Michigan State University Center for Advanced Microscopy. To prepare porous gel samples for SEM imaging, the samples were first freeze dried in an Electron Microscopy Sciences Model EMS750X freeze dryer (Electron Microscopy Sciences, Hatfield, PA). After cutting, they were mounted on aluminum stubs using carbon suspension cement (SPI Supplies, West Chester, PA) and adhesive tabs (M.E. Taylor Engineering, Brookville, MD). Then the samples were coated with osmium (about 10 nm thickness) in a Tennant20 osmium CVD (chemical vapor depositor) coater (Meiwafosis Co., Ltd., Osaka, Japan). These porous gel samples were examined in a JEOL 6610LV (tungsten hairpin emitter) scanning electron microscope (JEOL Ltd., Tokyo, Japan). Energy dispersive X-ray spectroscopy (elemental analysis) was done using an Oxford Instruments Aztec system (Oxford Instruments, High Wycomb, Bucks, England), software version 3.1 using a 20 mm^2 Silicon Drift Detector (JEOL 6610LV SEM) and an ultra-thin window.

2.2.5 Statistical analysis

Statistical analysis was performed using RStudio (version 2023.12.1) with R package (4.2.0). ANOVA and Tukey multiple comparison tests were conducted to assess differences in amino acid concentrations between the MAASS liquid absorbent and the porous gel + MAASS absorbent.

2.3 RESULTS

2.3.1 Porous gel expansion during desorption

An immediate observation when using the porous gel pieces was that during the desorption process, porous gel pieces expanded more quickly than the gel pieces soaked in MAASS at room temperature during absorbent material preparation. During the room temperature absorption preparation, gel pieces typically absorbed about 1 mL of MAASS per hour. However, with the heating of porous gels in MAASS during desorption, gel pieces gained between 4 mL and 8 mL of MAASS over the 45-minute period. This range in uptake volume could be influenced by the initial size of the gel piece and by the size of other gel pieces in the beaker for desorption. However, an article by Ahmed states that hydrogels have changes in volumetric capacity based on various physical or chemical stimuli, one of which is temperature (Ahmed, 2015). Thus, the increase of MAASS absorption capacity in the gel is likely a result of the porous gel's reaction to the physical stimuli of temperature. Higher temperatures increase the elasticity of the gel, allowing it to expand more easily. This increases absorption capacity for MAASS in the porous gel piece. Therefore, porous gel pieces exposed to MAASS at higher temperatures have a faster MAASS absorption rate into the gel.

2.3.2 MAASS material analysis

Characteristics of the MAASS were also analyzed in depth to further elucidate the reasoning behind its efficient CO_2 absorption capacity. Carbohydrate analysis results from the University of Georgia Complex Carbohydrate and Research Center were unexpected. The GC chromatograms resulting from glycosyl composition analysis showed the presence of amino acids, fatty acids, and the internal standards used, but no carbohydrates. The size exclusion chromatography gave inconclusive results. The salt peak was lower than expected considering

the large amount of salt in the MAASS from the addition of KOH, and the other peaks did not show signals from carbohydrates in the composition analysis. H-NMR analysis showed no observable signals from carbohydrates in two of the peaks and only a few very minor peaks within the remaining peak that could have been from carbohydrates. Overall, the analysis indicated no evidence for significant carbohydrate presence in the MAASS. The provided report on the results predicted this may be caused by carbohydrate degradation during KOH hydrolysis in the MAASS, resulting from a peeling reaction (a successive β-elimination reaction from the reducing end) (Stetten & Katzen, 1961).

LCMS amino acid analysis was first performed on the MAASS during processing. Samples were taken post-Parr reactor treatment and at the end of all MAASS processing steps. Amino acid levels in the solution were all higher at the end of processing due to residual solids from the lysed algae cells being spun out of the solution. This leaves the amino acids from the algae cells within the MAASS as the vital components used in CO_2 absorption reactions.

Amino acid analysis was performed again after running 10% and 50% CO_2 absorption trials. The MAASS used for these trials was compared to a separate container of MAASS that had been stored since the end of processing. The MAASS in use had much lower concentrations of amino acids than the stored MAASS. Based on these results, it was hypothesized that the porous gel may be selectively absorbing more amino acids than other components within the MAASS, creating a discrepancy in amino acid levels between the liquid MAASS and the MAASS absorbed within the porous gel.

To further clarify this difference, kinetics were run on the amino acid levels in MAASS during uptake into porous gel pieces. Two porous gels were placed in a beaker containing 100 mL of MAASS. The beaker was heated at about 95°C and every 30 minutes a sample was taken

from the MAASS liquid in the beaker. A replicate beaker was run following the same procedure. A total of 8 samples were taken from each beaker, with the first sample taken before the start of soaking. These samples were tested using LCMS to compare the concentration of amino acids in the porous gel over the soaking period.

ANOVA was performed to compare the concentrations of amino acids in the porous gel to the initial concentration of amino acids in the MAASS. The p-values from each amino acid ANOVA are given in column 2 of Table 1. These results indicated that 6 of the 13 amino acids present in MAASS had significantly different concentrations ($p<0.05$) in the MAASS within the porous gel compared to the control MAASS liquid. The p-value comparing the combined total amino acid concentration in the gel and in the control MAASS is 0.0523, which does not reach the desired significant p-value of 0.05, but is significant at the lower confidence p-value of 0.1. The general trend for each amino acid was a higher concentration in the porous gel than in the control MAASS liquid. Column 3 of Table 1 gives the ANOVA p-values for comparing amino acid concentrations in the porous gel at different stages of gel soaking/different volumes of MAASS in the gel. Glycine and lysine were the only amino acids to have significantly different concentrations ($p<0.05$) of amino acids in the porous gel across gel volumes during soaking. These amino acids appear to have a slight increase in concentration within the porous gel as it uptakes more MAASS.

Table 1. p-values for amino acid level comparisons in gel.

Amino Acid	p-values from ANOVA of control AA vs. gel AA	p-values from ANOVA comparing gel AA levels
Alanine	0.0437	0.239
Aspartic acid	0.0243	0.0703
Isoleucine	0.175	0.484
Glutamic acid	0.158	0.135
Glycine	0.0629	0.0331
Leucine	0.0228	0.508
Lysine	0.0343	0.0127
Methionine	0.363	0.0913
Phenylalanine	0.765	0.63
Proline	0.0124	0.107
Tryptophan	0.452	0.3
Tyrosine	0.0244	0.0877
Valine	0.089	0.484
Total AA	0.0523	0.16

Sections A.2 and A.3 in the appendix show the figures comparing individual amino acid concentrations between the gel and liquid and between the different gel sizes respectively. Figures 4 and 5 show these comparisons for total amino acids.

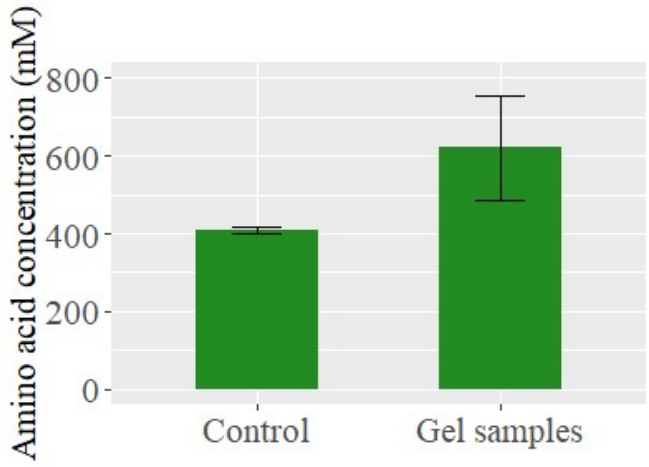

Figure 4. Amino acid concentration in the gel vs. in the control liquid.

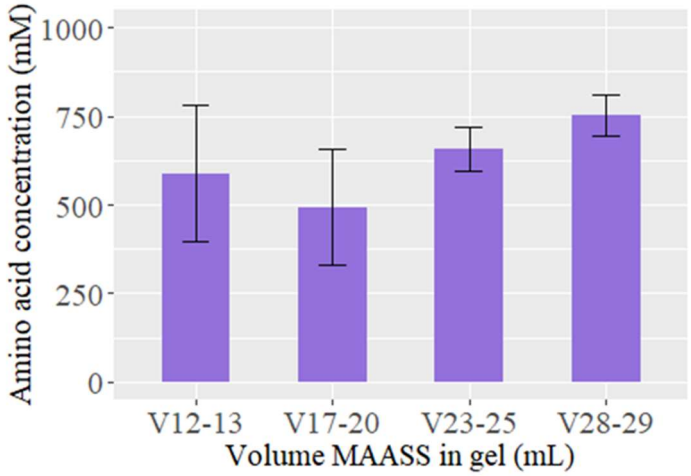

Figure 5. Amino acid concentrations in the gel at different gel sizes.

Overall, more individual amino acid concentrations are significantly different between the gel and liquid than between the different gel sizes. Since this significance shows higher concentrations of amino acids in the gel than in the liquid MAASS, porous gel pieces demonstrate some extra affinity for absorbing amino acids from the MAASS compared to other elements within MAASS. Given the results from comparing amino acid concentrations across gel sizes, this affinity is also relatively consistent across the entire gel soaking period.

2.3.3 SEM imaging of porous gel

SEM imaging was done on an initial porous gel piece, a porous gel piece swollen with 14 mL of water, a porous gel piece swollen with 4 mL of MAASS, and a porous gel piece swollen with 20 mL MAASS. Both pieces containing MAASS were imaged after undergoing CO_2 absorption. For each gel piece, imaging was done on the outer shell, the surface of one of the inner pores, and a cross section of the interior. The images of the cross sections were the most representative of the distinctness of each porous gel piece. Images of the initial gel piece were difficult to interpret due to the collapsed structure from the final drying step in the production process. However, Figure 6, the interior of the water swollen gel piece, clearly shows the structure of the gel with the pores expanded. Figure 7 shows the same interior perspective and magnification for the small algal swollen gel piece. In this image, it appears the MAASS has filled up many of the pores, with only a few openings still visible in the cross section. In Figure 8, the large algal swollen gel piece, none of the pores are visible. The gel piece appears to be completely saturated, with a biofilm of the MAASS visible in this cross section. The differences in pore visibility between these images illustrate the process of the porous gel piece becoming completely saturated with MAASS as it absorbs a larger volume and swells in size. As the pores become fuller, the gel piece expands in size to accommodate more liquid.

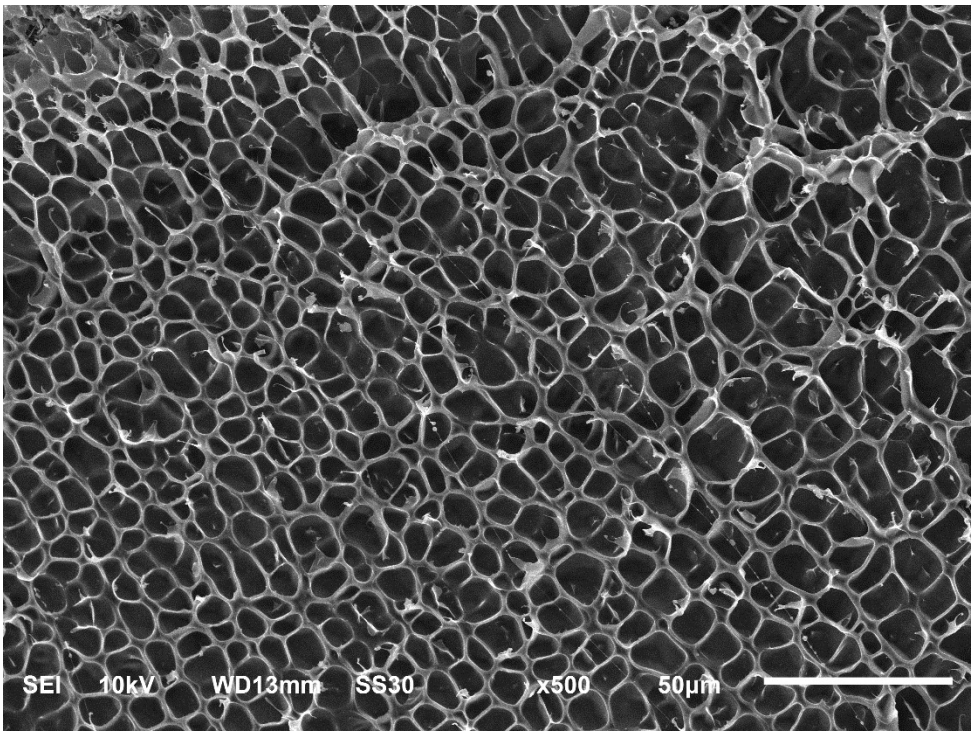

Figure 6. Cross section of water swollen porous gel piece.

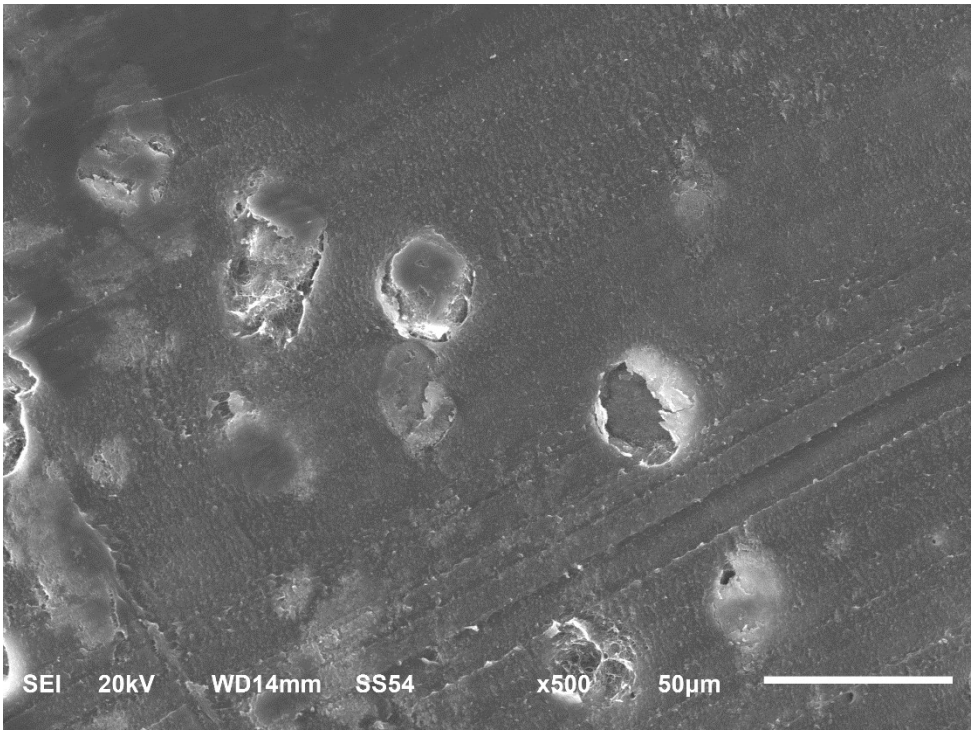

Figure 7. Cross section of small algal swollen porous gel piece.

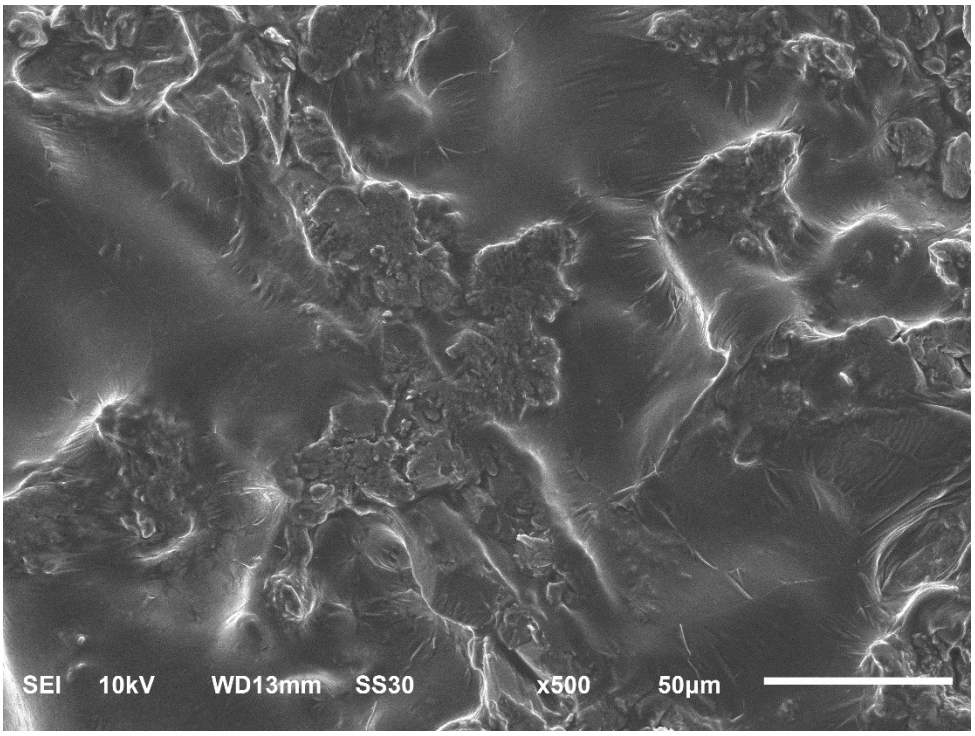

Figure 8. Cross section of large algal swollen porous gel piece.

In some gel pieces, crystallization appeared after the CO_2 absorption process. This was likely due to the presence of potassium salts within the solution. Figure 9 shows a view of the crystallization on the small algal swollen gel piece. These crystals were only found in images of the external shell of the gel piece. Interestingly, crystallization did not seem to influence the absorption capacity of the gel pieces. This may be because heating for the desorption process reduced the presence of these crystals between absorption runs.

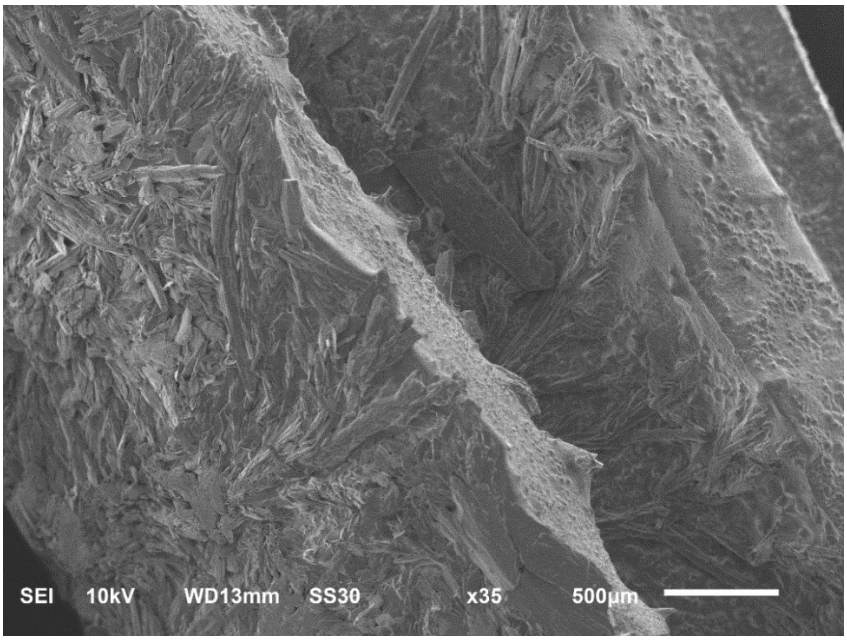

Figure 9. Crystallization on shell of small algal swollen porous gel piece.

EDX analysis was performed on some of the porous gel sections to determine the elements present in the material. Figure 10 gives the EDX spectrum for the cross section of the large algal swollen gel piece. Looking at the elements present in each gel piece, the cross section of the water swollen gel piece contained about 58% carbon, 23% oxygen, and 20% nitrogen by weight. In comparison, the small algal swollen gel piece had only 46% carbon and 12% nitrogen, but 28% oxygen and 13% potassium by weight. The presence of potassium confirms that MAASS is present inside the gel. The increased levels of oxygen are likely due to both the presence of amino acids from the MAASS in the gel and to the presence of carbon dioxide absorbed within the gel piece. The profile of elements in the large algal swollen gel piece is almost the same as the small algal swollen gel piece, with 28% carbon, 4% nitrogen, 42% oxygen, and 25% potassium by weight. The similar profiles between the algal swollen gel pieces indicate that the amount of MAASS within a given porous gel piece may be proportional to the CO_2 absorbed within that piece.

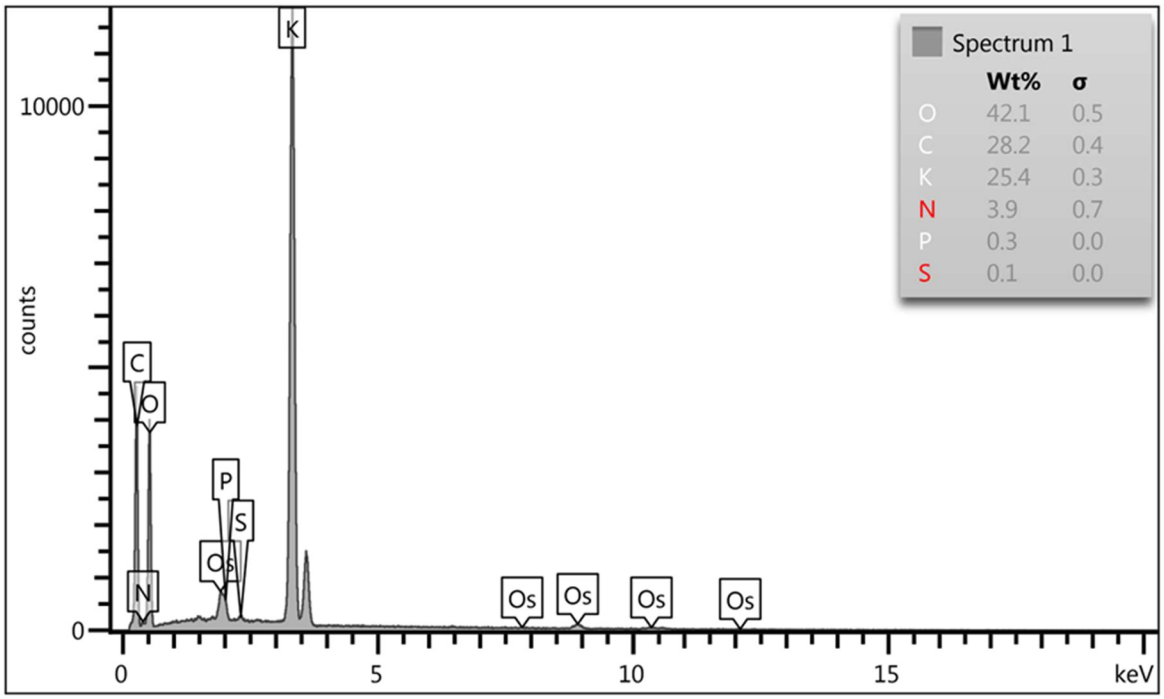

Figure 10. EDX spectrum from cross section of large algal swollen porous gel piece.

2.4 CONCLUSIONS

Table 2 provides a summary of the material composition of the MAASS based on the testing performed. The makeup of the MAASS is mostly amino acids and KOH, with negligible presence of carbohydrates found. Future analysis should be performed to analyze the MAASS for the presence of other components that may affect the CO_2 absorption potential.

Table 2. Material composition of the MAASS.

Material type	**Presence in MAASS**
Carbohydrates	Negligible
Total amino acids	422.5 +/-23 mM
Potassium	8% (Wt%) (Smerigan et al., 2023)

CHAPTER 3: CARBON DIOXIDE ABSORPTION USING MICROALGAL AMINO ACID SALT SOLUTION HELD IN POROUS DOUBLE NETWORK GEL

3.1 INTRODUCTION

This chapter focuses on calculating and analyzing the CO_2 absorption capacity of MAASS held in porous gel. Different volumes of MAASS are compared to elucidate how the size of the porous gel affects absorption rate and capacity. This includes employing multi-objective optimization as a tool to optimize the CO_2 absorption process using the combined porous gel + MAASS material. In addition, a mass and energy balance is performed to characterize the CO_2 absorption process. A life cycle analysis discusses the impact of the proposed absorption system over its lifetime.

3.2 MATERIALS AND METHODS

3.2.1 Absorption

Once the porous gel + MAASS material is assembled, the absorption setup is prepared. Compressed gas cylinders purchased from Airgas were used for controlled delivery of carbon dioxide to the absorption material. The concentrations tested were 10% CO_2, 30% CO_2, and 50% CO_2, with air as the balance gas. The compressed gas cylinder is connected to the reactor setup located inside the fume hood. This setup contains in series a bubble gas flowmeter, an Omega FMA-LP1620A-V2 digital gas flow meter, a 250 mL Pyrex glass bottle as the reactor, and a Leaton dual-port QX-1201 digital manometer for measuring differential pressure. A Dwyer U-inclined analog manometer was also used for initial testing of the absorption setup. The connections between equipment are made using silicon tubing with an 1/8-inch inner diameter and 1/4-inch outer diameter, and all connections are airtight. An ICUM9000EA 3-way Lopez T-

valve is used to connect a Quantek Instruments Model 908 IR CO_2 Gas Analyzer between the glass reactor and manometer. The T-valve can be used to control which of the three connections are open with a rotating closure for one closed outlet at a time. Another T-valve is also placed between the digital flowmeter and the glass reactor. Figure 11 illustrates this absorption setup with an overall view on the left and a larger view of the components inside the fume hood on the right.

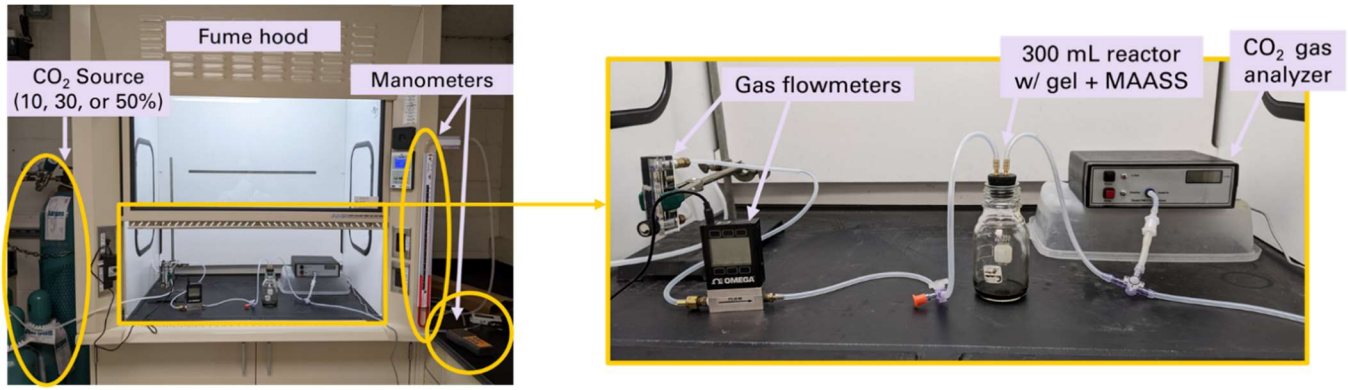

Figure 11. Carbon dioxide absorption setup inside the fume hood.

To start the experiment, the glass reactor is flooded with the gas from the compressed gas cylinder at a flowrate of about 1 L/min. The first T-valve is open between the digital gas flowmeter and glass reactor. The second T-valve is opened to the glass reactor and CO_2 gas analyzer only, with the manometer connection closed. The gas is set to flow through at about 1 L/min until the CO_2 gas analyzer reading stabilizes at a percentage of CO_2 close to that of the compressed gas cylinder being used. Then the gas flow is briefly turned off, and the connection to the digital manometer is opened to fill the tubing between the reactor and manometer with the correct CO_2 concentration. The connection is then switched back to the CO_2 gas analyzer and the gas flow is resumed.

At this point, the tubing connection to the CO_2 gas analyzer is opened to the atmosphere and the gas flowrate is increased to about 2 L/min. The opened connection occurs because the CO_2 gas analyzer cannot receive a gas flowrate higher than 1 L/min without risk of damage. While this connection is open, the reactor is quickly opened and the absorbent material (MAASS liquid or porous gel + MAASS) is placed inside. The reactor is quickly shut, and after about 10 seconds the gas flow is reduced to about 1 L/min again. The tubing is reconnected between the reactor and CO_2 gas analyzer.

When the CO_2 gas analyzer shows a percentage of CO_2 close to that of the compressed gas cylinder being used, the compressed gas cylinder is closed. The time between adding the absorbent material and closing the gas cylinder is about 60 seconds on average. The T-valves are quickly adjusted so that the first connection is closed and there is no open connection for gas to leave the reactor. The second T-valve is open only between the glass reactor and manometer. These changes ensure that the reactor is closed to all entities except the manometer.

At this point, the changing readings on the manometer are monitored and recorded to determine the change in pressure within the glass reactor. The absorption trial concludes when the manometer reading is stable and no longer changing, or when the cutoff time is reached.

Control trials were performed for 10% CO_2 and 50% CO_2 using an equivalent volume of MAASS as the volume of MAASS absorbed by the porous gel pieces used in the experimental trials. This included trials for 4, 8, 12, 16, and 20 mL of MAASS. The volume of MAASS absorbed into and held in the gel is difficult to control, especially during the desorption process, but the same number of trials was performed as for the control MAASS trials with a similar distribution of MAASS volume across the trials. Triplicates were performed to collect data from 15 MAASS absorption trials and 15 porous gel + MAASS absorption trials. The same number of

trials were performed for each CO_2 concentration (10%, 30% and 50% by volume).

3.2.2 Desorption

To regenerate the absorbent material for reuse in subsequent trials, desorption is performed. The desorption process is done using a reflux device, shown in Figure 12. The absorbed MAASS is placed within a glass beaker, and the gel pieces containing MAASS are placed within this solution. The beaker is placed on the hot plate and connected to the condenser above, which has cold water continuously flowing through it as the coolant source. This prevents water evaporation from the MAASS during heating. The hot plate is set for heating at a low level to prevent damage to the porous gel pieces. Temperature is monitored using a Ryobi IR002 infrared thermometer. After about 45 minutes, the hot plate is turned off, and after about 15 more minutes, the beaker is removed from the hot plate for cooling. The cold-water source and reflux device are turned off. After cooling, the pH of the MAASS can be measured to confirm desorption of CO_2 from the MAASS (pH of about 10). At this point, the absorbent material is ready for reuse in another absorption trial.

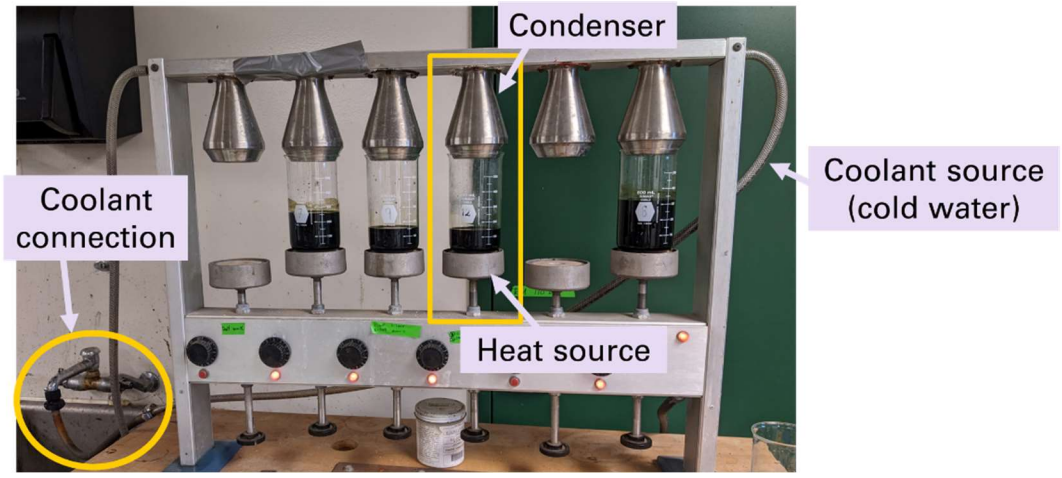

Figure 12. Reflux device used for desorption setup.

3.2.3 Calculating CO_2 absorption capacity

To analyze the acquired data on absorption capacity for each trial, several calculations are performed. First, the recorded initial concentration of CO_2 in the reactor is used to calculate the moles of CO_2 in the reactor. The readings from the digital manometer give the change in pressure in the reactor (inH_2O). The calculated pressure vacuum within the reactor post-absorption is assumed to be solely from CO_2 being absorbed into the MAASS. Therefore, the ideal gas equation (PV=nRT) was used to calculate the moles of CO_2 present in the reactor post-absorption using this measured pressure change. Thus, the calculated difference in moles of CO_2 within the reactor pre- and post-absorption is the moles of CO_2 absorbed by the MAASS. This value can be converted to mL of CO_2 absorbed using the ideal gas equation. A sample calculation of CO_2 absorption capacity is given in Appendix A.1. Any absorption of CO_2 during storage of the porous gel + MAASS pieces between absorption trials is not considered in this calculation. Since gel pieces are stored in small, sealed beakers, potential absorption of CO_2 during storage was calculated to be less than 0.05 mL CO_2/gel.

3.2.4 Statistical analysis

Statistical analysis was performed using MATLAB (version R2023b) and RStudio (version 2023.12.1) with R package (4.2.0). The curve fitting tool in MATLAB was used to fit the data to the pseudo-first order absorption kinetics model given in equation 1. Equation 2 shows this equation after being solved. Pseudo-first order absorption kinetics was selected for analysis due to the known importance of absorption rate and absorption volume in optimizing CO_2 absorption within the MAASS. For each absorption trial, the time (t) and absorption (V) data were input into equation 2 to solve for the CO_2 absorption constant (k_{ab}) and equilibrium absorption volume (V_{eq}). A normalized version of the absorption data was used, where the CO_2

absorption amount (V) at each time was recorded in mL CO_2 absorbed/mL MAASS. All of the k_{ab} and V_{eq} values calculated for each trial using the curve fitting tool had an R^2 value >0.99.

$$\frac{dV}{dt} = k_{ab}(V_{eq} - V)$$

(Eq. 1)

$$V = V_{eq}(e^{-k_{ab}t} + 1)$$

(Eq. 2)

Using the values of k_{ab} and V_{eq} calculated for each trial, the data were grouped into categories based on volume of MAASS used in each trial. The chosen categories were 4-6 mL, 8-13 mL, 14-19 mL, and 20-23 mL of MAASS. These categories were selected so that the data points were relatively evenly distributed across the categories for all CO_2 concentrations used. ANOVA and Tukey multiple comparison tests were then conducted to assess differences between the MAASS liquid absorbent and the porous gel + MAASS absorbent. ANOVA analysis was used to compare absorption constants and equilibrium absorption volume for trials with and without porous gel. Pair-wise comparisons were performed to compare absorption trends for different volumes of MAASS used.

3.2.5 Mass and energy balance

Based on the experimental results, mass and energy balance calculations were conducted on the porous gel + MAASS CO_2 absorption system using a 100 MW natural gas power plant (T.B. Simon Power Plant, East Lansing, MI) for reference. This power plant generates 360,100 metric tons of CO_2 per year, with flue gas containing 10% (v/v) carbon dioxide. The system boundary for this analysis includes a MAASS production unit and the porous gel + MAASS CO_2

capture unit. Preparation of the combined porous gel + MAASS absorbent material occurs on-site. The CO_2 absorption capacity of the porous gel + MAASS material is used to determine the scale of algal cultivation needed for biomass production.

3.3 RESULTS

3.3.1 Carbon dioxide absorption at 10% CO_2 concentration

For the carbon dioxide absorption trials run at 10% CO_2 concentration by volume, each trial was cut off at a maximum of 60 minutes. Since a small volume of CO_2 was initialized in the reactor (about 30 mL), MAASS was not fully saturated with CO_2 at the end of these absorption trials. As previously mentioned, control scenarios were performed using only MAASS as the absorbent material. Figure 13 shows the results of the absorption trials for the 10% CO_2 concentration. Only the median trial for each testing condition was graphed to more clearly illustrate the differences in CO_2 absorption between the liquid MAASS and porous gel + MAASS. The difference in curve shape between the control trials and the trials using MAASS held in porous gel indicates a different rate of absorption. Final CO_2 absorption capacity appears to be similar across all trials.

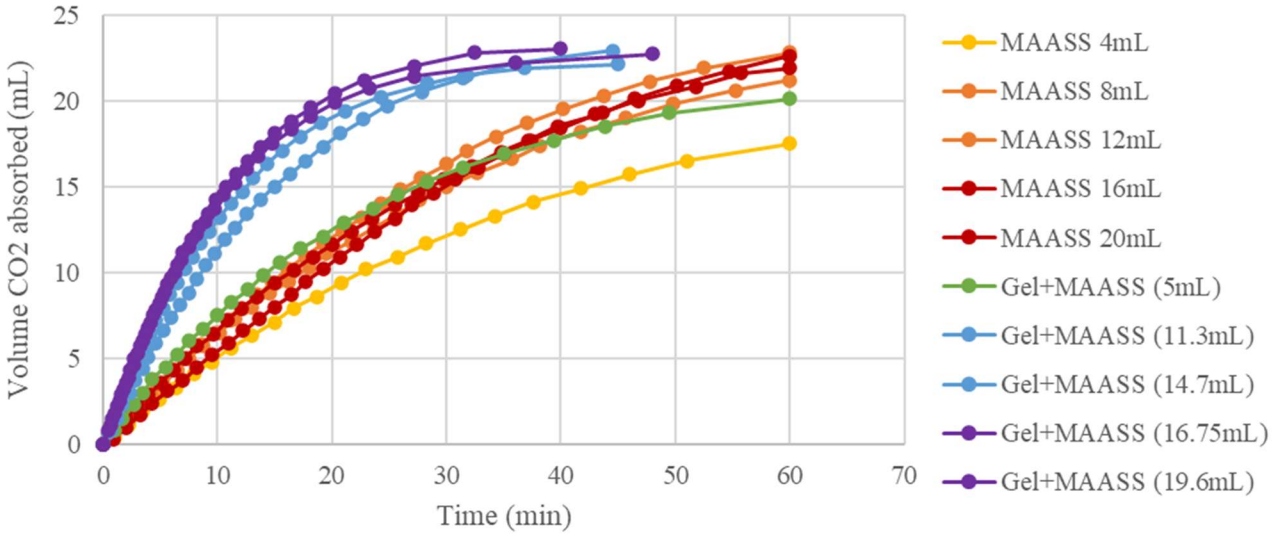

Figure 13. Select results from 10% CO_2 absorption - CO_2 absorbed.

Figure 14 shows the absorption capacity for each trial when it is normalized on a volumetric basis. The same median trials from Figure 13 are used in this graph. Looking at this perspective, absorption trials using a smaller volume of MAASS have a larger normalized absorption capacity than the larger volumes of MAASS.

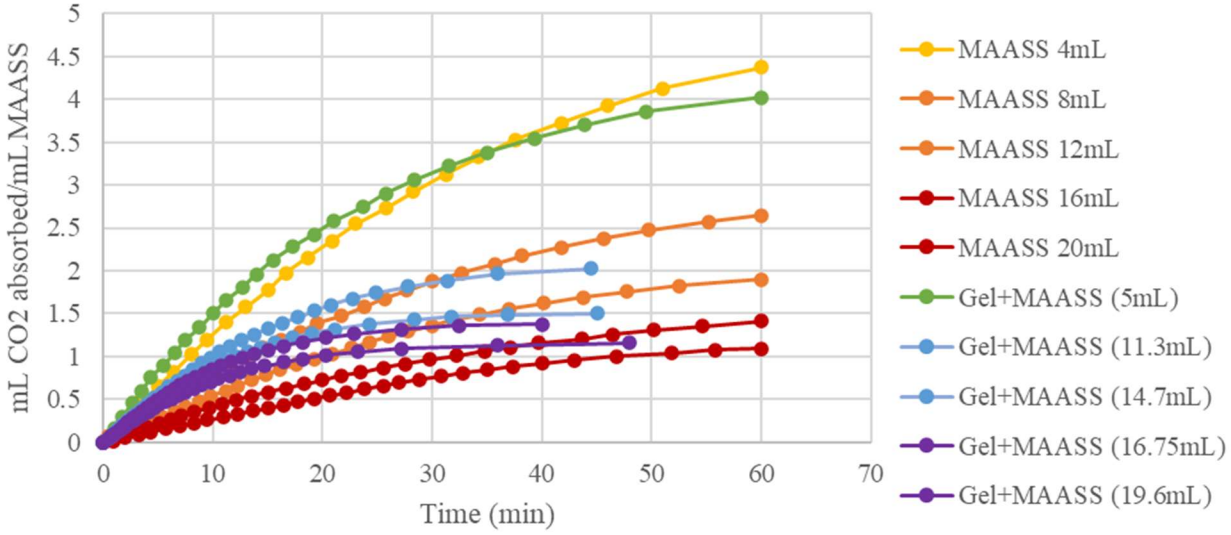

Figure 14. Select results from 10% CO_2 absorption - CO_2 absorbed/mL MAASS.

A two-way ANOVA was run to compare calculated CO_2 absorption constant (k) values for each trial with respect to the volume of MAASS and whether porous gel was used during absorption. K-values were found to be significantly different ($p<0.05$) between absorptions with and without porous gel, and significantly different ($p<0.05$) between volumetric categories of MAASS used. This confirms the observations from Figure 13. In addition, Tukey pair-wise comparisons showed k-values for the 4-6 mL MAASS volumetric category to be significantly different ($p<0.05$) than the other 3 volumetric categories. However, none of the other pairwise comparisons of k-values between volumetric categories were significantly different.

A separate two-way ANOVA was run to compare calculated CO_2 equilibrium absorption volumes (V_{eq}) across all trials. V_{eq} represents the normalized CO_2 absorption measurements in mL CO_2 absorbed/mL MAASS. V_{eq} values were also found to be significantly different ($p<0.05$) between absorptions with and without porous gel, and significantly different ($p<0.05$) between volumetric categories of MAASS used. However, there was no significant difference between V_{eq} values when considering both factors simultaneously. Tukey pair-wise comparisons for this test showed significant differences ($p<0.05$) in V_{eq} values between all MAASS volumetric category comparisons except between the 14-19 mL category and 20-23 mL category.

Focusing on the absorption trials without porous gel, a one-way ANOVA showed k-values to not be significantly different between MAASS volumetric categories, but the V_{eq} values were significantly different ($p<0.05$) between all categories except for between 14-19 mL and 20-23 mL categories.

For the absorption trials using porous gel, however, the one-way ANOVA indicated k-values to be significantly different ($p<0.05$) between MAASS volumetric categories. Tukey pair-wise comparisons showed this significance when comparing the 4-9 mL category to all other

categories, similar to the statistical results for k-values when comparing all absorption trials. V_{eq} values had the same pattern of significant differences as the k-values from these trials.

The R-generated figures illustrating the differences in k-values and V_{eq} values based on porous gel usage and MAASS volumetric categories are supplied in Appendix A.4.1. Appendix A.5 gives the R code used for statistical analysis of absorption trials at each concentration of CO_2. Overall, at 10% CO_2 concentration by volume, the absorption rate is significantly faster when using porous gel pieces, with a smaller difference when comparing equilibrium absorption volume. This indicates porous gel pieces to be the optimal absorbent material at 10% CO_2 concentration by volume. However, maximizing the absorption rate and equilibrium absorption volume for the porous gel is dependent on the volumetric category, with different optimal volumes for each factor.

2.3.2 Carbon dioxide absorption at 30% CO_2 concentration

For the carbon dioxide absorption trials run at 30% CO_2 concentration by volume, each trial was cut off at a maximum of 60 minutes. Again, due to the low volume of CO_2 initialized in the reactor (about 90 mL), MAASS was not saturated with CO_2 at the end of these absorption trials. Control trials were not performed for 30% CO_2 concentration by volume because the control trials from the minimum (10%) and maximum (50%) CO_2 concentrations were deemed to provide sufficient information for analysis. The CO_2 absorption results for the median of each testing condition at 30% CO_2 concentration are given in Figure 15. These results follow a similar trend to the results from 10% CO_2 concentration, but with the different testing conditions having a larger range of final CO_2 absorption volumes. In addition, the smallest volume of MAASS used in the porous gel + MAASS trials (about 4 mL) had a noticeably smaller absorption capacity than the other trials containing larger volumes of MAASS.

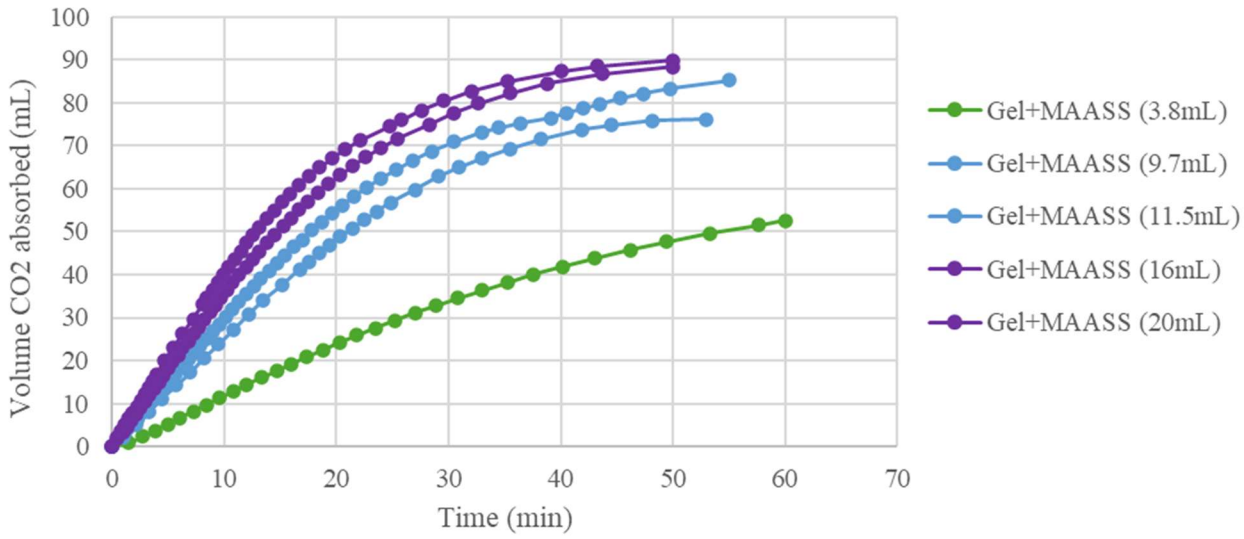

Figure 15. Select results from 30% CO_2 absorption - CO_2 absorbed.

Figure 16 shows the absorption capacity for each trial when it is normalized on a volumetric basis, using the same median trials from Figure 15. The trend is similar to that of the normalized 10% CO_2 concentration trials, with the smaller volumes of MAASS having an increased normalized CO_2 absorption capacity compared to the larger volumes of MAASS.

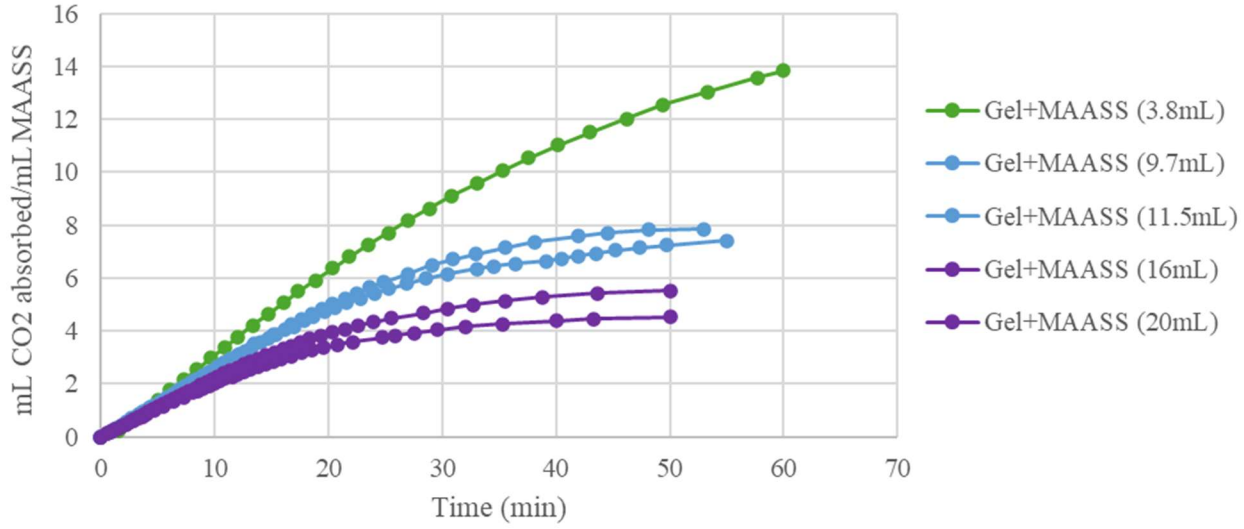

Figure 16. Select results from 30% CO2 absorption - CO2 absorbed/mL MAASS.

At 30% CO_2 absorption, only the one-way ANOVAs were run for the k-value and V_{eq} value because all absorption trials used porous gel. The ANOVA comparing k-values showed the k-values to be significantly different ($p<0.05$) both between all MAASS volumetric categories and for each pair-wise comparison between MAASS volumetric categories. For V_{eq} values, the ANOVA across all MAASS volumetric categories was also significant. Pair-wise comparisons showed V_{eq} values between all volumetric categories to be significant ($p<0.05$) except for the comparison between the 14-19 mL and 20-23 mL volumetric categories. Thus, maximizing the absorption rate and equilibrium absorption volume at 30% CO_2 concentration by volume also appears to be dependent on the volumetric category. However, the optimal volume of MAASS is still different when maximizing each factor. Appendix A.4.2 shows the R-generated plots of k-values and V_{eq} values across MAASS volumetric categories.

2.3.3 Carbon dioxide absorption at 50% CO_2 concentration

For the carbon dioxide absorption trials run at 50% CO_2 concentration by volume, each trial was cut off at a maximum of 75 minutes. This total time was increased from the previous trials in order to visualize the same portion of the absorption curve, due to the larger volume of CO_2 and slower absorption rate in these trials. Results for the median of each testing condition are given in Figure 17. Trials at this concentration of CO_2 have the greatest range in final volume of CO_2 absorbed. This is likely caused by more of the trials reaching CO_2 saturation in the MAASS compared to the trials at 10% and 30% CO_2 by volume. Similar to the other CO_2 concentrations, the porous gel + MAASS trials at 50% CO_2 concentration have a higher rate of absorption than the MAASS control trials, especially at the start of absorption.

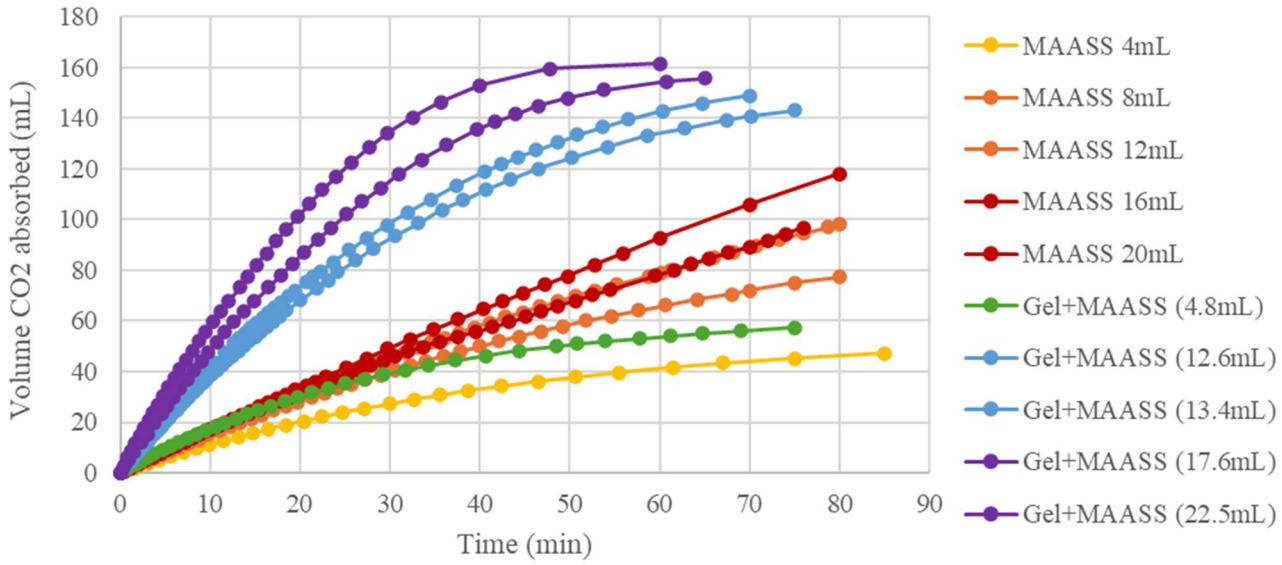

Figure 17. Select results from 50% CO_2 absorption - CO_2 absorbed.

Figure 18 shows the normalized CO_2 absorption capacity for each trial, using the same median trials from Figure 17. The trials containing smaller volumes of MAASS still have the largest normalized absorption capacity for 50% CO_2 concentration. However, the gel trials containing larger volumes of MAASS have similar normalized absorption capacity to the control MAASS trials with smaller volumes of MAASS.

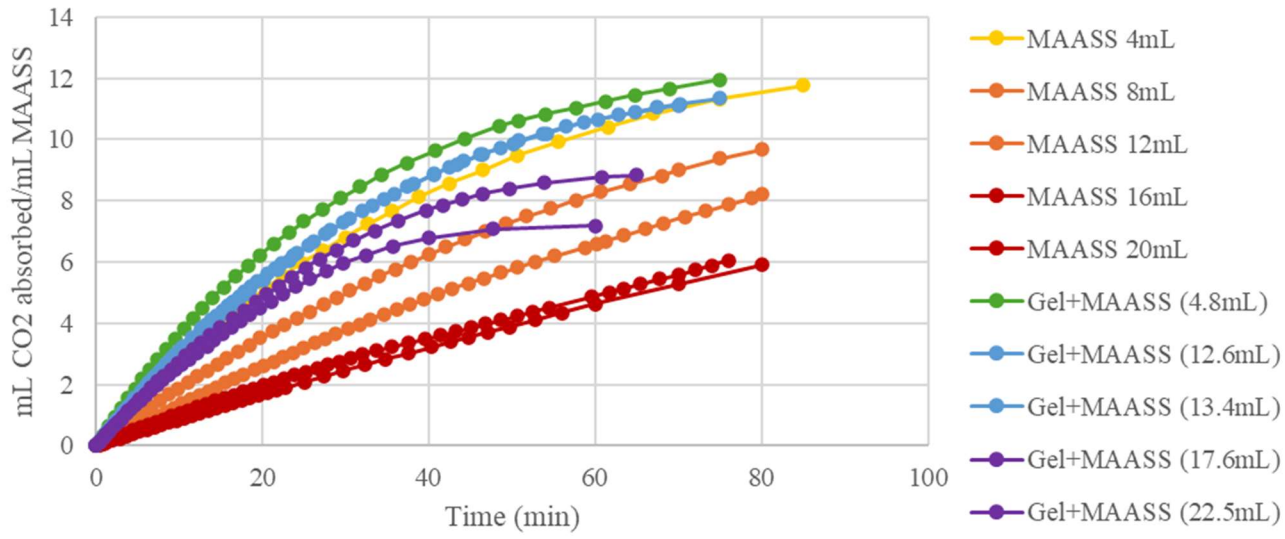

Figure 18. Select results from 50% CO_2 absorption - CO_2 absorbed/mL MAASS.

A two-way ANOVA was run to compare k-values from each trial against MAASS volumetric categories and porous gel usage. K-values were found to be significantly different ($p<0.05$) both between MAASS volumetric categories and between absorption trials with and without porous gel. Tukey pair-wise comparisons showed k-values for the 4-6 mL volumetric category to be significantly different ($p<0.05$) from the other 3 volumetric categories.

The two-way ANOVA comparing V_{eq} values did not show significant difference in V_{eq} values across only MAASS volumetric categories or only absorption trials with and without porous gel. However, V_{eq} values were significantly different ($p<0.05$) when considering both factors simultaneously. None of the pair-wise comparisons showed significantly different ($p<0.05$) V_{eq} values between specific MAASS volumetric categories or between absorption trials with and without porous gel.

One-way ANOVA for absorption trials without porous gel showed k-values to be significantly different ($p<0.05$) across MAASS volumetric categories. Tukey pair-wise

comparisons again showed k-values for the 4-6 mL volumetric category to be significantly different ($p<0.05$) from the other 3 volumetric categories. The one-way ANOVA and Tukey pair-wise comparisons both showed no significant difference in V_{eq} values across MAASS volumetric categories.

For absorption trials with porous gel, the one-way ANOVA showed k-values to be significantly different ($p<0.05$) across all MAASS volumetric categories. The following Tukey pair-wise comparisons also had significantly different k-values: 4-6 mL & 8-13 mL, 4-6 mL & 20-23 mL, 8-13 mL & 20-23 mL, and 14-19 mL & 20-23 mL. For V_{eq} values, the one-way ANOVA showed significant difference ($p<0.05$) across MAASS volumetric categories. All Tukey pair-wise comparisons showed significantly different ($p<0.05$) V_{eq} values except for the comparison between the 4-6 mL and 8-13 mL volumetric categories.

Appendix A.4.3 shows the R-generated plots of k-values and V_{eq} values across MAASS volumetric categories and absorption trials with and without gel. Overall, porous gel absorption trials have a significantly larger absorption rate at 50% CO_2 concentration by volume, with equilibrium absorption volume not being significantly different based on porous gel usage. This further supports the conclusion of combining MAASS and porous gel for the optimal absorbent material. Again, optimizing the absorption rate and equilibrium absorption volume for these gel trials is dependent on the volumetric category and yields different optimal values for each factor.

2.3.4 Multi-objective optimization

All three of the tested CO_2 concentrations support the conclusion that using the combined porous gel + MAASS material offers optimal CO_2 absorption conditions. However, optimizing absorption is dependent on multiple factors. In this study, CO_2 concentration (by volume) in the absorption environment, absorption rate (k), equilibrium absorption volume (V_{eq}), and MAASS

volume used were determined to be the most important factors influencing absorption. As mentioned in the methods section, these known factors of importance influenced selection of the kinetics equation, since they were the variables that would eventually be optimized. There may be other variables influencing CO_2 absorption, but since their presence and effect are unknown, optimization will be based on the four factors listed above.

When considering these variables, they do not have the same correlations affecting absorption capacity. For example, smaller volumetric categories of MAASS correlate to increased CO_2 equilibrium absorption volume, while larger volumetric categories of MAASS correlate to increased absorption rate. Thus, multi-objective optimization is needed to determine the optimal conditions for CO_2 absorption. The goal of this optimization is to maximize the absorption rate, maximize the equilibrium absorption volume, and minimize the MAASS volume used. In addition, since this study is focused on an industrial scenario where flue gases have a CO_2 concentration of about 10% by volume, the optimization was also run to minimize the CO_2 concentration in the absorption environment.

Initially, 3D Pareto fronts were graphed in RStudio for each CO_2 concentration using CO_2 absorption constant (/min), CO_2 equilibrium absorption volume (mL CO_2/mL MAASS), and MAASS volume in gel (mL) as the axes. For each figure, a 3D nonlinear regression model was generated using the exponential function given in Equation 3, where x is the CO_2 absorption constant (/min), y is the CO_2 equilibrium absorption volume (mL CO_2/mL MAASS), and z is the MAASS volume in the gel (mL).

$$z = d + a * \exp\left(b * x + c * y\right)$$

(Eq. 3)

The parameters a, b, c, and d were generated iteratively to determine the best fit for each data set. The generated parameter values followed by their corresponding p-values are given in Table 3. Figures 19-21 show the 3D pareto front for each CO_2 concentration with their calculated 3D nonlinear regression model. The R code used for 3D Pareto analysis is given in Appendix A.6.

Table 3. Generated parameter values for the regression equation at each CO_2 concentration.

	a	p-value	b	p-value	c	p-value	d	p-value
10% CO_2	117.824	0.199	-10.434	0.106	-0.990	0.004	4.010	0.026
30% CO_2	42.649	0.136	-2.815	0.751	-0.143	0.040	1.852	0.478
50% CO_2	-0.005	0.821	79.630	0.036	0.430	0.098	24.749	0.001

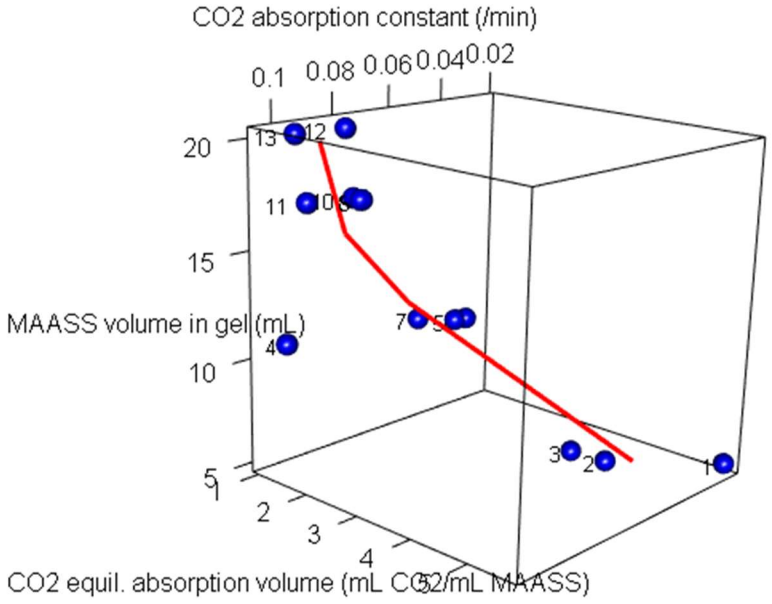

Figure 19. Pareto front and nonlinear regression line for 10% CO_2 concentration.

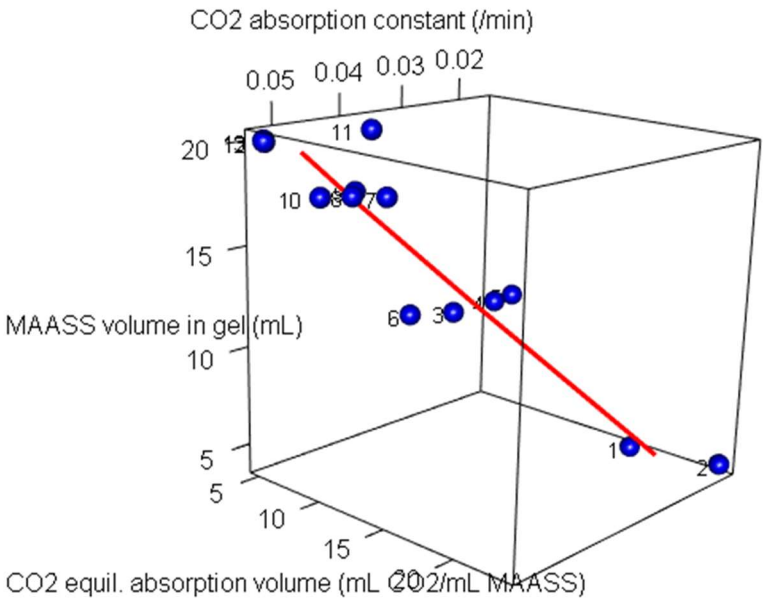

Figure 20. Pareto front and nonlinear regression line for 30% CO_2 concentration.

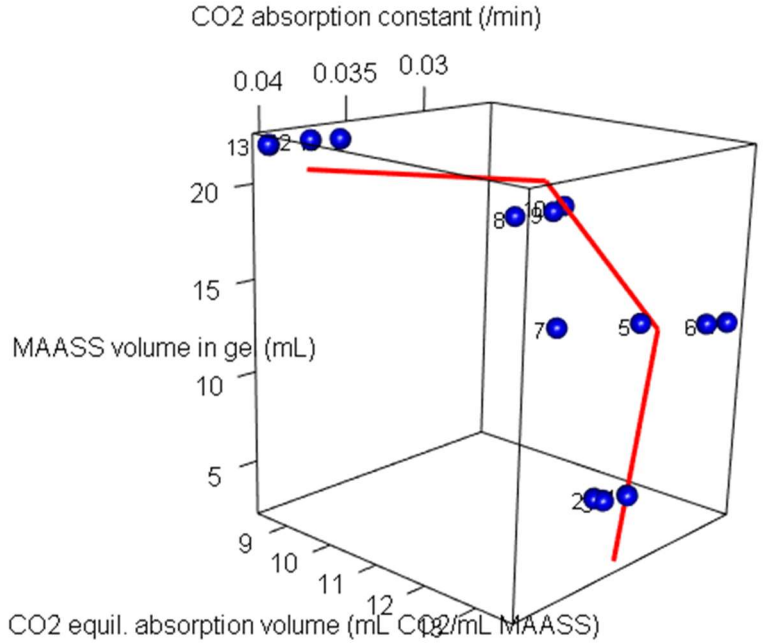

Figure 21. Pareto front and nonlinear regression line for 50% CO_2 concentration.

These plots and regression lines for each CO_2 concentration show different relationships between the factors on each axis. To determine which points on each regression line represent the optimum CO_2 absorption conditions, further analysis needs to be performed. For this next step, Non-dominated Sorting Genetic Algorithm (NSGA) version II is used to determine the optimal conditions across all 4 parameters.

NSGA is a popular method for multi-objective optimization that is used when optimizing one objective hurts another objective's optimization. First, the initial population of candidate solutions is generated. In this case, the average values for absorption constant and equilibrium absorption volume were calculated for the MAASS volumetric categories of 4-6 mL, 8-13 mL, 14-19 mL, and 20-23 mL. This was done for each CO_2 concentration used, resulting in 11 total values for the initial population. Next, each value, also called a candidate solution, is evaluated for its fit with the optimization objectives. The three objectives considered for this project are to maximize absorption rate, maximize equilibrium absorption volume, and minimize MAASS volume used.

After establishing the initial population for NSGA, iterations are performed using this initial population by combining pairs of solutions to create new solutions or by mutating values slightly to create new solutions. This results in the generation of suggested optimal solutions that balance the chosen objectives. For this analysis, a final population size of 12 was selected for the suggested solutions, and 100 generations of solution sets were created iteratively to optimize these solution values. The R-code used for this NSGA analysis is given in Appendix A.7. As the solution populations are generated, the best solutions are selected to move on to the next generation based on crowding distance and whether solutions are non-dominated or not. A larger crowding distance is preferable, where a solution is farther from neighboring solutions. Solutions

are also ranked by how many other solutions they are dominated by, with non-dominated solutions being the most preferable. Elitism is also used to make sure that the best solutions are retained throughout subsequent generations of solution sets. The final population contains a diverse set of solutions with the best possible tradeoffs between objectives. Figure 22 shows the 3D Pareto front with these 12 suggested solutions from the NSGA analysis. To consider all 4 parameters, the NSGA analysis was run to maximize the absorption rate, maximize the equilibrium absorption volume, and minimize the MAASS volume used. Then when selecting the best solutions from the NSGA final population, solutions that minimize CO_2 content in the absorption environment will be prioritized.

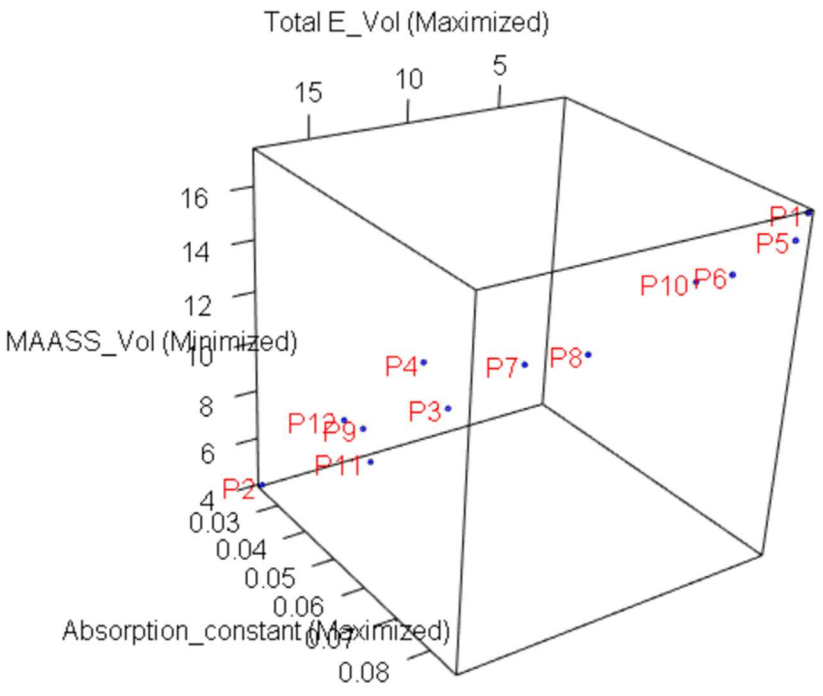

Figure 22. Suggested multi-objective optimization solutions from the NSGA analysis.

At this point, the final set of solutions is manually examined to decide which choices are the best at balancing the desired objectives. This depends on which factor should be the most optimized, which in this case will be minimizing the CO_2 content in the absorption environment. This study seeks to optimize CO_2 absorption in flue gas, so the lowest CO_2 concentration meets this scenario. Table 4 gives the average parameter values for each solution in the final set.

Table 4. Optimized parameter values for the final set of solutions from the NSGA analysis.

	CO_2 equilibrium absorption volume (mL CO_2/mL MAASS)	CO_2 absorption constant (/min)	MAASS volume in gel (mL)
Solution 1	1.27	0.0868	17.3
Solution 2	17.52	0.0231	4.0
Solution 3	11.30	0.0461	8.2
Solution 4	11.98	0.0420	9.8
Solution 5	1.35	0.0853	16.2
Solution 6	3.08	0.0790	14.7
Solution 7	9.28	0.0569	10.5
Solution 8	6.83	0.0619	10.9
Solution 9	14.06	0.0356	6.9
Solution 10	3.86	0.0739	14.2
Solution 11	13.29	0.0335	5.1
Solution 12	14.81	0.0340	7.3

The solutions provided in the final set that most equally optimize the three parameters while also minimizing the CO_2 content in the absorption environment are solutions 3, 4, 7, 9, and 11. The most highly ranked data point from the initial population that contributes to each of these solutions is data point 2 for solution 3, data point 5 for solution 4, data point 2 for solution 7, data point 4 for solution 9, and data point 4 for solution 11.

Therefore, data points 2 and 4 represent the overall optimal condition for CO_2 absorption. These data points represent CO_2 absorption using a porous gel containing 8-13 or 20-23 mL of MAASS with 10% CO_2 concentration by volume in the absorption environment. In conclusion, any further CO_2 absorption testing for flue gas should use 8-13 or 20-23 mL of MAASS at 10% CO_2 concentration by volume to achieve optimal absorption rate and volume. Since it is more resource-effective to use less MAASS, using a smaller volume within this range would be ideal.

2.3.5 Mass balance

A mass balance was performed using the defined system boundary, shown in Figure 23. These calculations show that high-rate algal photobioreactors with a volume of 12,365 m^3 are needed to produce the required amount of MAASS to capture 90% of CO_2 emissions from the power plant. The flue gas (containing 986,575 kg CO_2/day) is pumped through the photobioreactor to provide CO_2 for algal growth. A small portion of this CO_2 (62 kg/day) in the flue gas is used by the algae. The rest of the CO_2 from the flue gas (986,513 kg/day) is passed through for CO_2 capture by the porous gel + MAASS material. Algal cultivation requires an average of 198 m^3/day of water, 332 kg/day of nitrogen, and 75 kg/day of phosphorus. The retention time for algal cultivation is 0.5 days, so 6,182 m^3 of the culture broth is harvested each day. After harvesting, 49,460 kg/day of wet biomass with a moisture content of 25% and 5,984 m^3 recycled water is generated.

The wet algal biomass is further processed by an alkali hydrolysis process using a thermal reactor to produce the microalgal amino acid salt solution (MAASS) (Smerigan et al., 2023). The MAASS has an amino acid concentration of 46 g/L and a potassium concentration of 79 g/L. The combined porous gel + MAASS absorbent material is then prepared as described in the previous sections. The final amino acid concentration in the gel was 65 g/L.

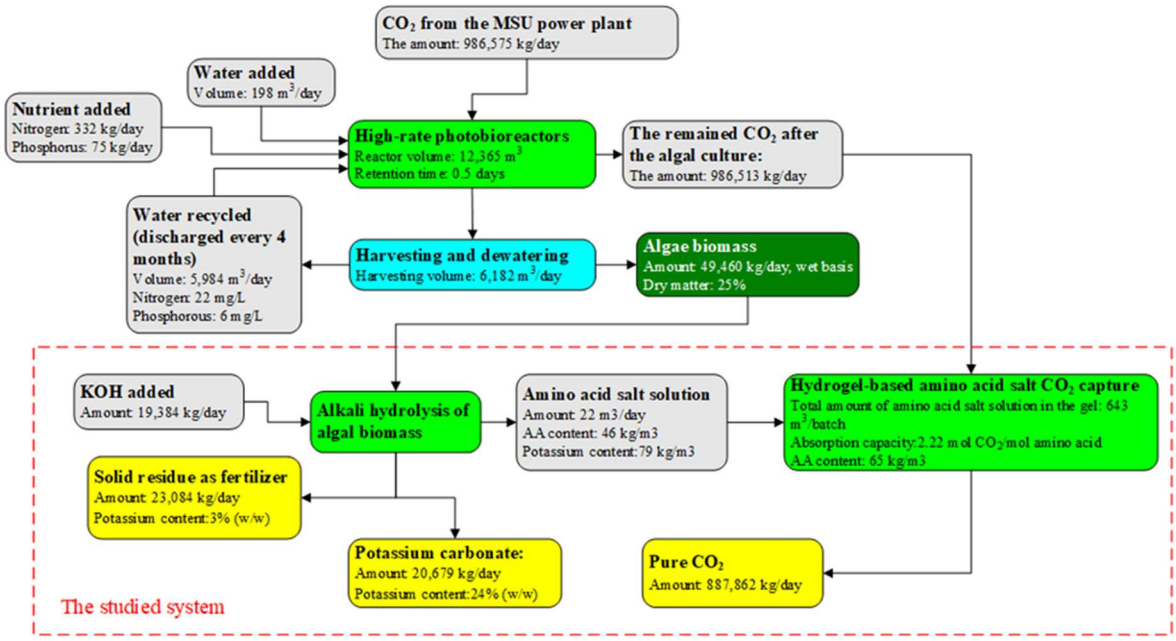

Figure 23. Mass balance of the integrated algal cultivation and porous gel + MAASS CO2 absorption process on a 100 MW natural gas power plant.

An absorption and subsequent desorption stripping process is used for CO_2 capture with the porous gel + MAASS material. The optimized absorption capacity of this material is 2.24 mol CO_2/mol amino acid. For this analysis, the absorption and desorption time is set at 60 minutes/circle (10 minutes of absorption and 50 minutes of desorption). Considering a lifetime of 1,000 cycles of CO_2 absorption for the porous gel + MAASS material (Smerigan et al., 2023), 1 m^3/day of fresh MAASS is needed to maintain CO_2 capture potential. Table 5 compares the mass flow of porous gel + MAASS absorbent with the liquid MAASS absorbent. Compared to liquid MAASS by itself, the current study reduces the required amount of MAASS by 20% to capture the same amount of CO_2 from the power plant. Meanwhile, the photobioreactor volume needed to produce the required algal biomass for the porous gel + MAASS material was 20% smaller than the volume needed for using the MAASS liquid by itself. This significantly improves space issues encountered with algal cultivation.

Not only does the porous gel + MAASS material significantly improve the efficiency of CO_2 capture, but it also reduces the size of the algal cultivation process. This demonstrates a promising combination of biological and chemical approaches to develop a new, efficient CO_2 capture process.

Table 5. Comparison of porous gel + MAASS absorbent with liquid MAASS absorbent [a].

	Porous gel + MAASS absorbent material	Liquid MAASS absorbent material
Preparation of the algal amino acid salt solution		
The required new MAASS (m^3/day) [b]	22	27
Amino acid concentration in the material (kg/m^3)	65	65
K in the solution (kg/m^3)	79	79
Algal cultivation		
Volume of photobioreactors (m^3)	12,365	15,454
CO_2 capture		
Captured CO_2 from the power plant (metric ton/day)	887	888

a. The same 100 MW natural gas power plant was used for both cases. The data for the liquid MAASS absorbent was obtained from a previous study (Smerigan et al., 2023).
b. Needed to maintain CO_2 capture potential based on a porous gel + MAASS material lifetime of 1,000 cycles of CO_2 absorption.

2.3.6 Energy balance

The energy balance for this CO_2 absorption system is presented in Table 6. The porous gel + MAASS absorbent was compared with both liquid MAASS and monoethanolamine (MEA) processes based on the 100 MW natural gas power plant. These results show that the porous gel + MAASS scenario requires 906,719 and 1,881,921 MJ/day of electricity and heat respectively to capture 90% of CO_2 in the flue gas. Considering the electricity (8,640,000 MJ/day) and heat (21,600,000 MJ/day) generation of the power plant, this equates to only 10% and 9% of electricity and heat generated from the power plant.

Comparatively, the liquid MAASS absorption system requires 12% and 15% of electricity and heat inputs, and the MEA absorption system requires 10% and 20% of the electricity and heat outputs of the power plant. In this scenario with the MSU power plant used in the mass and energy balance, excess heat generated by the power plant is needed to heat campus infrastructure. Therefore, this heat is not considered for recycled use within the absorption systems. Thus, the studied porous gel + MAASS system has better overall energy performance than the liquid MAASS and conventional MEA absorption processes.

Table 6. Comparison of energy demands between three systems to capture CO_2 from a 100 MW natural gas power plant [a].

	Energy input (MJ/day)		
System components	**Porous gel + MAASS absorbent [b]**	Liquid MAASS absorbent [c]	MEA absorbent [d]
Algae cultivation			
CO_2 delivery (electricity) [e]	**147,986**	147,986	-
Algal cultivation operation (electricity) [f]	**7,048**	8,809	-
Preparation of MAASS [g]			
Electricity energy	**73**	89	
Heat energy	**5,390**	6,615	
CO_2 capture [h]			
CO_2 capture (electricity) [i, j]	**751,612**	912,323	887,918
CO_2 capture (heat) [k]	**1,876,531**	3,270,067	4,173,215
Total electricity input	**906,719**	1,069,207	887,918
Total heat input	**1,881,921**	3,276,682	4,173,215
Total energy input	**2,788,640**	4,345,889	5,061,133

a. The energy balance is calculated based on the 100 MW natural gas power plant. The energy input is assigned as negative. The energy output is assigned as positive.
b. The proposed system consists of algae photobioreactor cultivation, MAASS production, and porous gel + MAASS CO_2 capture.
c. The proposed system consists of algae photobioreactor cultivation, MAASS production, and liquid MAASS CO_2 capture.
d. The MEA CO_2 capture process consumes 1 MJ/kg CO_2 captured of electricity and 4.7 MJ/kg CO_2 captured of heat.
e. The energy for CO_2 delivery is 0.15 MJ/kg CO_2 delivered. 986,575 kg/day of CO_2 was delivered though the algae cultivation.

Table 6 (cont'd)

f. The photobioreactor cultivation operation includes mixing, pumping, make-up water delivery, on-site circulation, and dewatering. The power demand for these operations is 0.57 MJ/m^3/day (Clippinger & Davis, 2019). The volumes of the photobioreactors for the porous gel + MAASS absorption and liquid MAASS absorption are 12,365 m^3 and 15,454 m^3, respectively.
g. The electricity and heat demands for the preparation of MAASS were 3.3 and 245 MJ/m^3 solution respectively based on data from a previous study (Smerigan et al., 2023). The volumes of MAASS for the porous gel absorbent and liquid absorbent are 22 and 27 m^3/day, respectively.
h. The volume of MAASS per batch for the porous gel absorbent and liquid absorbent are 643 m^3 and 2,241 m^3, respectively.
i. Two Sulzer axial flow pumps (1,200 kW and 45,000 m^3/hr each) are used as the feeding pumps to circulate the absorbent for the liquid MAASS. The circulation flow rate is 69,753 m^3/hour based on the gas/absorbent volume ratio of 3:1.
j. Four Lamson 960 blowers (2,910 kW and 70,000 m^3/hr each) are used to pump the flue gas to the absorption towers for both porous gel + MAASS absorption and liquid MAASS absorption.
k. The thermal energy required for desorption is calculated using the heat equation. The parameters are as follows: the initial temperature of the absorbent is 20ºC and the desorption temperature is 100ºC. The specific heat capacity of the MAASS is 3.8 kJ/kg/K. The heat recovery efficiency of desorption is 60%.

2.3.7 Life cycle analysis

Life cycle assessment for these absorption systems was focused on global warming potential (GWP), water eutrophication potential, and water use. Corresponding impact categories were analyzed using contribution analysis (Chen et al., 2015). The global warming potential is the amount of greenhouse gases that is potentially released in a year. The power plant with 100 MW capacity generates 360,100 metric ton/year of CO_2, which has a GWP of 360,100 metric ton/year. For both the MAASS and MEA processes, uncaptured CO_2 and energy consumption contribute to GWP. The value of 0.117 kg CO_2 emitted/MJ energy is used to calculate GWP from energy consumption. Considering emissions from uncaptured CO_2 and energy consumption from the CO_2 capture process, the porous gel + MAASS absorption system has a GWP of 75,706 metric ton/year of CO_2. This eliminates 79% of GWP from power plant emissions, which is

better than the liquid MAASS scenario with a GWP reduction of 73%, and much better than the MEA scenario with a GWP reduction of 70%.

For water eutrophication potential, the chemicals used for the MEA process do not have a negative impact, unlike the MAASS systems that use N and P as nutrients for algal cultivation. The unit for water eutrophication potential is metric ton PO_4-e/year. The conversion factors for TN and TP are 0.42 kg PO_4-e/kg TN and 3.07 kg PO_4-e/kg TP respectively according to the EPA Tool for Reduction and Assessment of Chemicals and Other Environmental Impacts (TRACI 2.1). Due to low nutrient concentration in the discharged water (22 mg/L of N and 6 mg/L of P), the eutrophication potentials of the porous gel + MAASS system and the liquid MAASS system are 598 and 479 kg PO_4/year respectively, which is relatively low.

However, water usage for the liquid MAASS and porous gel + MAASS systems has a relatively large impact. This is something that should be considered and minimized in future development of this system. Since the porous gel + MAASS system is more efficient and therefore needs less fresh algae biomass each day, the water use is lower for this system. It requires 72,270 metric tons/year of water compared to 90,155 metric tons/year for the liquid MAASS system, which is a 20% reduction. Figure 24 and Table 7 show the contribution analysis for the selected impact categories, compared across the absorption scenarios.

This life cycle impact assessment demonstrates that the porous gel + MAASS system significantly reduces GWP from power plant emissions and has a lower overall impact, which indicates that algal cultivation combined with porous gel + MAASS CO_2 capture could make a major contribution to the power industry by capturing CO_2 in a technically sound, economically feasible, and environmentally friendly way.

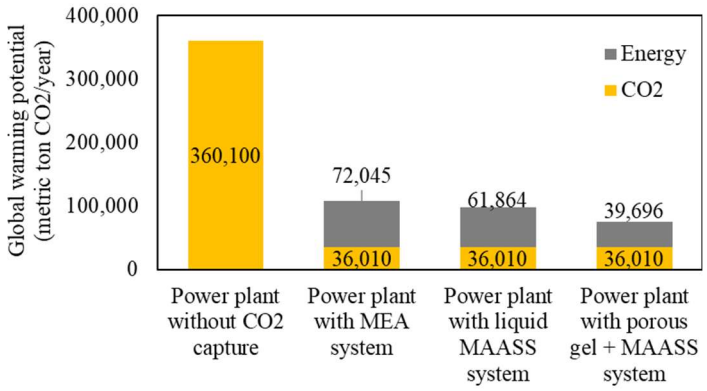

A

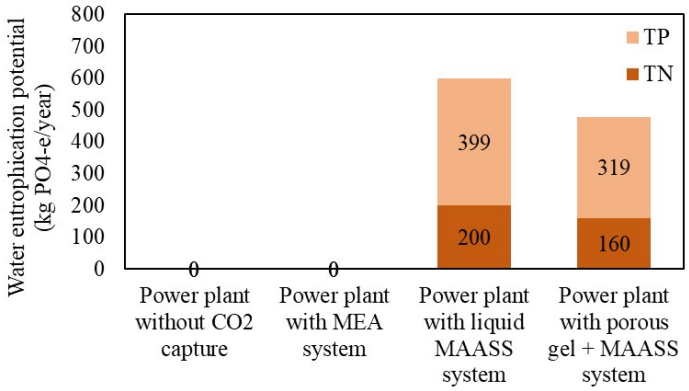

B

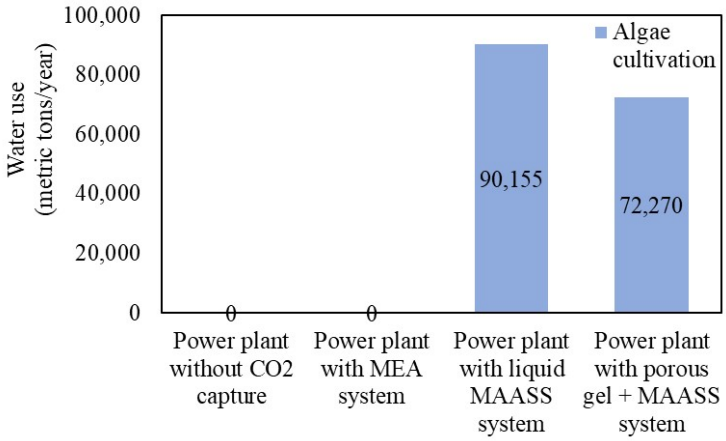

C

Figure 24. Contribution analysis of individual impact categories for the studied CO_2 capture system. A) Global warming potential; B) Water eutrophication potential; C) Water use.

Table 7. Comparison of life cycle impact assessment across absorption scenarios.

	Power plant (no CO_2 capture)	Power plant with MEA system	Power plant with liquid MAASS system	Power plant with porous gel + MAASS system
Global warming potential (metric ton CO_2-e/year)	360,100	108,055	97,874	75,706
Water eutrophication potential (kg PO_4-e/year)	0	0	598	479
Water Use (metric tons/year)	0	0	90,155	72,270

CHAPTER 4: CONCLUSIONS AND FUTURE WORK

4.1 ABSORPTION COLUMN REACTOR

The end goal of this research is to develop an industrial scale absorption column to be co-located at a power plant for CO_2 absorption from flue gases. The next step towards this goal is to test CO_2 absorption with multiple gel pieces in a column. Multi-objective optimization of absorption conditions concluded that using 8-13 or 20-23 mL of MAASS at 10% CO_2 concentration by volume would result in the optimal absorption rate and volume. Using a smaller volume of MAASS would also be resource effective. So, for the initial testing of a column-type setup, 4 porous gel pieces were used for absorption at these conditions. Each of these pieces contained 10-13 mL of MAASS, with a combined total of 44 mL of MAASS used in the column.

A similar absorption setup to the other absorption experiments was used. However, instead of using a digital manometer to measure pressure difference, the reactor was connected solely to the CO_2 gas analyzer to measure changes in CO_2 concentration in the reactor. In addition, there was a continuous flow of about 0.1 LPM of gas containing 10% CO_2 into the reactor column.

First, an empty bottle was connected to the system and the gas flowrate was set to approximately 0.1 LPM. Next, the empty bottle was switched out with the bottle containing the porous gel pieces swollen with MAASS. Then the percentage of CO_2 in the reactor output was continuously recorded for at least 30 minutes until the CO_2 concentration equalized. Gas flowrate was monitored over the absorption period to ensure its stability. Figure 25 shows this setup for column absorption trials. Three absorption trials were run using the same porous gel pieces each time, with one control trial run using an empty bottle in place of the bottle containing porous gel + MAASS.

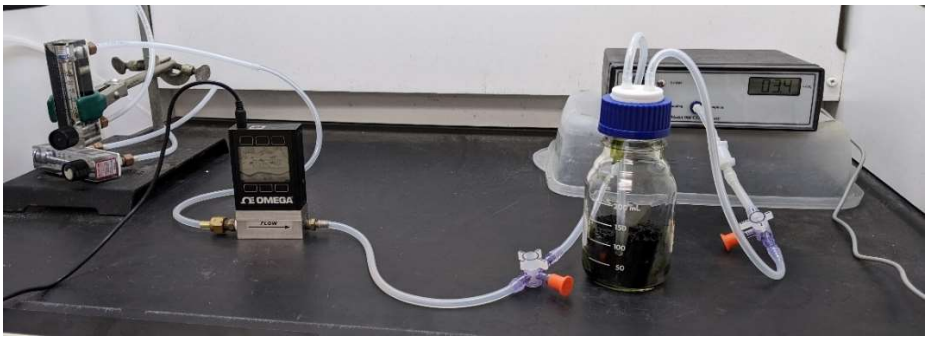

Figure 25. Column absorption setup.

Figure 26 shows the trend of CO_2 concentration in the reactor output for the control run and for the three absorption trials. None of the absorption trials reached the expected equilibrium value of 9% CO_2 from the provided gas input during the trial period. After the third absorption, the gas flow was left running for a total absorption time of 3 hours, and the output CO_2 concentration continued to increase slowly up to a final value of 7.4% CO_2. It is possible that the MAASS may continue slowly absorbing CO_2 during this period. Alternatively, the high density of CO_2 compared to other elements present in the air may cause the CO_2 to stick to the bottom of the reactor instead of reaching the output for gas flow at the top of the reactor.

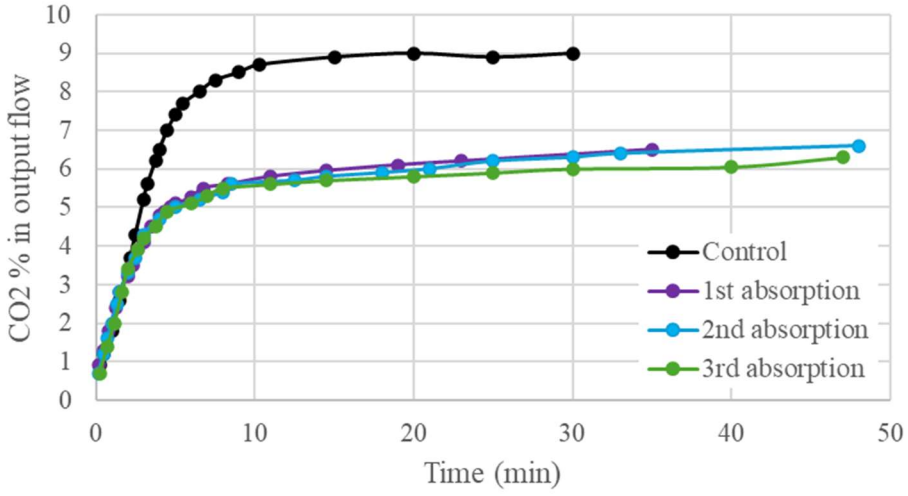

Figure 26. Percent CO_2 in output for each column absorption trial.

To regenerate the MAASS for each absorption run, the bottle containing the porous gel + MAASS pieces was autoclaved at 100ºC for one hour, releasing the steam pressure at the end to clear the desorbed CO_2 from the autoclave. Then the process was repeated for a second one-hour autoclave period. After cooling, the reactor was ready for the next absorption trial. This new desorption method was used to maintain the same volume of MAASS in the gel, as opposed to the previous method where porous gel pieces were heated within MAASS liquid for desorption. It was first tested using a single gel piece, and the absorption capacity was found to be consistent in absorption trials run before and after autoclaving. In future work, a similar heating method to an autoclave can be used to maintain the volume of porous gel pieces within the reactor across absorption runs.

For the first absorption trial run using the column setup, the overall absorption capacity was calculated to be 1.02 L of CO_2. On a volumetric basis, this capacity was calculated to be 0.96 mol CO_2 absorbed/L of MAASS. Calculations were performed in MATLAB (Version R2023b) using curve fitting and the integration function. The MATLAB code used for this analysis is provided in Appendix A.8.

The second absorption trial had an overall absorption capacity of 0.99 L of CO_2 and a capacity of 0.92 mol CO_2 absorbed/L of MAASS on a volumetric basis. The third absorption trial had an overall absorption capacity of 0.99 L of CO_2 and a capacity of 0.93 mol CO_2 absorbed/L of MAASS on a volumetric basis. Over the three column absorption trials, the absorption capacity was very similar with non-significant degradation over time. On average, the absorption capacity of the column was 1.0 L of CO_2. This equates to 0.94 mol CO_2 absorbed/L of MAASS.

The MAASS used in this study has a total amino acid concentration of 422.5 +/-23 mM. Using this value, the molar absorption capacity is calculated to be 2.24 mol CO_2/mol amine when using MAASS held in porous gel. Comparing this to the previous absorption research using MAASS, MAASS liquid by itself was determined to have an absorption capacity of 1.27 mol CO_2/mol amine (Smerigan et al., 2023). Thus, using the combined medium of MAASS held in the porous gel improves the overall absorption capacity of the MAASS liquid by 75%. Figure 27 illustrates this difference in absorption capacity for different absorbent materials. This further proves the superior efficiency of porous gel + MAASS as an absorbent material compared to other existing options.

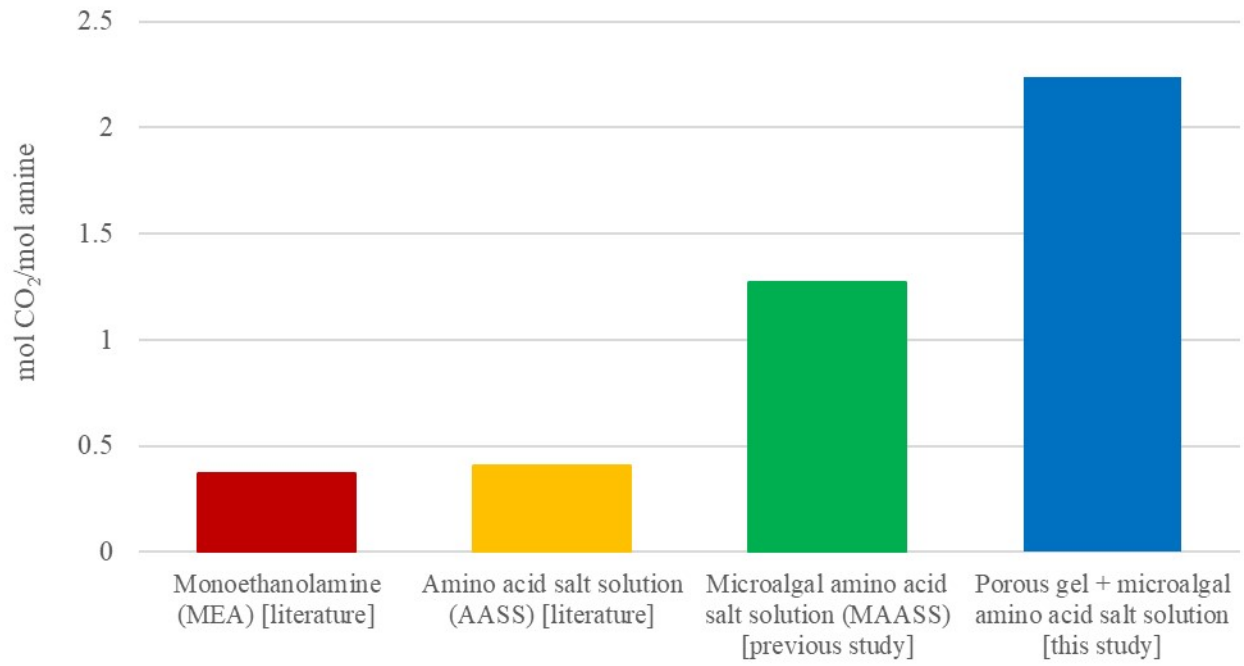

Figure 27. Comparison of molar absorption capacity across existing absorbent materials.

4.2 CONCLUSIONS

In conclusion, the combined porous gel + MAASS material was found to be effective, efficient, and sustainable as a CO_2 capture technology. Use of the porous gel eliminated issues

with foaming when using the liquid MAASS by itself. In addition, the increase in the exposed surface area while using the gel allowed for increased absorption of CO_2 when using larger volumes of MAASS, improving absorption capacity over previous absorbent materials. Material analysis indicated that porous gel selectively absorbs amino acids from the MAASS, further increasing CO_2 absorption efficiency compared to using MAASS liquid by itself. Multi-objective optimization of absorption conditions concluded that using 8-13 or 20-23 mL of MAASS at 10% CO_2 concentration by volume would result in the optimal absorption rate and volume. When using these conditions within a column absorption reactor setup, the molar absorption capacity of porous gel + MAASS was calculated to be 2.24 mol CO_2/mol amine. This capacity is 1.75x higher than using MAASS liquid by itself, and 5.6x higher than using popular absorbent materials such as MEA and synthetic AASS. In addition to this high absorption efficiency, the porous gel + MAASS material is sustainable due to its recyclability through the desorption process. Its recyclability and high absorption efficiency also contribute to a lower overall life cycle impact compared to other absorbent materials. Overall, this material has very strong potential as a CO_2 absorbent for future use at an industrial scale level.

4.3 FUTURE WORK

Further development of this system will focus on design of an industrial-scale absorption column that can capture carbon emissions from industrial sources such as power plants before they reach the atmosphere. To achieve this, the proposed column absorption system will need to be scaled up to an industrial level. Future research needs to be done on the use of porous gel pieces in a column format, and the best way in which to arrange them to prevent compaction and reduction of surface exposure to the CO_2 being absorbed. Further testing should also be done on heating methods for desorption when using a larger column format. Using a setup similar to an

autoclave would be optimal so that heating can occur without removing the porous gel pieces from the column. Excess heat generated by the industrial emissions source could also be used as a source for desorption heating. However, the ability to exhaust desorbed CO_2 should be considered when exploring desorption options. In addition, porous gel replacement methods should be investigated for when gel pieces within the column become damaged. Finally, a techno-economic analysis (TEA) should be performed once this industrial-scale absorption column is further developed to optimize the cost-effectiveness of the design. The purity of collected CO_2 from desorption should be measured to include potential reuse of CO_2 in this analysis.

REFERENCES

Ahmed, E. M. (2015). Hydrogel: Preparation, characterization, and applications: A review. *Journal of Advanced Research*, *6*(2), 105-121. https://doi.org/https://doi.org/10.1016/j.jare.2013.07.006

Alaswad, A., Dassisti, M., Prescott, T., & Olabi, A. G. (2015). Technologies and developments of third generation biofuel production. *Renewable and Sustainable Energy Reviews*, *51*, 1446-1460. https://doi.org/https://doi.org/10.1016/j.rser.2015.07.058

Aronu, U. E., Hoff, K. A., & Svendsen, H. F. (2011). CO2 capture solvent selection by combined absorption–desorption analysis. *Chemical Engineering Research and Design*, *89*(8), 1197-1203. https://doi.org/https://doi.org/10.1016/j.cherd.2011.01.007

Azzi, M., & White, S. (2016). Emissions from amine-based post-combustion CO2 capture plants. In P. Feron (Ed.), *Absorption-based post-combustion capture of carbon dioxide* (pp. 487-504). Woodhead publishing. https://doi.org/http://dx.doi.org/10.1016/B978-0-08-100514-9.00020-2

Baldev, E., Mubarakali, D., Saravanakumar, K., Arutselvan, C., Alharbi, N. S., Alharbi, S. A.,…Thajuddin, N. (2018). Unveiling algal cultivation using raceway ponds for biodiesel production and its quality assessment. *Renewable Energy*, *123*, 486-498. https://doi.org/https://doi.org/10.1016/j.renene.2018.02.032

Cheah, W. Y., Show, P. L., Chang, J.-S., Ling, T. C., & Juan, J. C. (2015). Biosequestration of atmospheric CO2 and flue gas-containing CO2 by microalgae. *Bioresource Technology*, *184*, 190-201. https://doi.org/https://doi.org/10.1016/j.biortech.2014.11.026

Chen, R., Rojas-Downing, M. M., Zhong, Y., Saffron, C. M., & Liao, W. (2015). Life cycle and economic assessment of anaerobic co-digestion of dairy manure and food waste. *Industrial Biotechnology*, *11*(2), 127-139.

Clippinger, J. N., & Davis, R. E. (2019). *Techno-economic analysis for the production of algal biomass via closed photobioreactors: future cost potential evaluated across a range of cultivation system designs*.

Cutshaw, A., Daiek, C., Zheng, Y., Frost, H., Marks, A., Clements, D.,…Clary, W. (2020). A long-term pilot-scale algal cultivation on power plant flue gas–Cultivation stability and biomass accumulation. *Algal Research*, *52*, 102115. https://doi.org/https://doi.org/10.1016/j.algal.2020.102115

EPA. (2024). *Inventory of U.S. Greenhouse Gas Emissions and Sinks: 1990-2022*. U.S. Environmental Protection Agency Retrieved from https://www.epa.gov/ghgemissions/inventory-us-greenhouse-gas-emissions-and-sinks-1990-2022

Harun, R., Yip, J. W. S., Thiruvenkadam, S., Ghani, W. A., Cherrington, T., & Danquah, M. K. (2014). Algal biomass conversion to bioethanol–a step-by-step assessment. *Biotechnology journal*, *9*(1), 73-86. https://doi.org/https://doi.org/10.1002/biot.201200353

Krsko, P., McCann, T. E., Thach, T.-T., Laabs, T. L., Geller, H. M., & Libera, M. R. (2009). Length-scale mediated adhesion and directed growth of neural cells by surface-patterned poly(ethylene glycol) hydrogels. *Biomaterials*, *30*(5), 721-729. https://doi.org/https://doi.org/10.1016/j.biomaterials.2008.10.011

Liu, Y., Wang, J., Chen, H., & Cheng, D. (2022). Environmentally friendly hydrogel: A review of classification, preparation and application in agriculture. *Science of The Total Environment*, *846*, 157303. https://doi.org/https://doi.org/10.1016/j.scitotenv.2022.157303

Luis, P. (2016). Use of monoethanolamine (MEA) for CO2 capture in a global scenario: Consequences and alternatives. *Desalination*, *380*, 93-99. https://doi.org/10.1016/j.desal.2015.08.004

Moreira, D., & Pires, J. C. M. (2016). Atmospheric CO2 capture by algae: negative carbon dioxide emission path. *Bioresource technology*, *215*, 371-379. https://doi.org/https://doi.org/10.1016/j.biortech.2016.03.060

Park, M.-R., Chun, C., Ahn, S.-W., Ki, M.-H., Cho, C.-S., & Song, S.-C. (2010). Sustained delivery of human growth hormone using a polyelectrolyte complex-loaded thermosensitive polyphosphazene hydrogel. *Journal of Controlled Release*, *147*(3), 359-367. https://doi.org/https://doi.org/10.1016/j.jconrel.2010.07.126

Pavlik, D., Zhong, Y., Daiek, C., Liao, W., Morgan, R., Clary, W., & Liu, Y. (2017). Microalgae cultivation for carbon dioxide sequestration and protein production using a high-efficiency photobioreactor system. *Algal Research*, *25*, 413-420. https://doi.org/https://doi.org/10.1016/j.algal.2017.06.003

Ramezani, R., Mazinani, S., & Di Felice, R. (2022). State-of-the-art of CO2 capture with amino acid salt solutions. *Reviews in Chemical Engineering*, *38*(3), 273-299. https://doi.org/https://doi.org/10.1515/revce-2020-0012

Saul, J. M., & Williams, D. F. (2011). 12 - Hydrogels in Regenerative Medicine. In K. Modjarrad & S. Ebnesajjad (Eds.), *Handbook of Polymer Applications in Medicine and Medical Devices* (pp. 279-302). William Andrew Publishing. https://doi.org/https://doi.org/10.1016/B978-0-323-22805-3.00012-8

Smerigan, A., Uludag-Demirer, S., Cutshaw, A., Marks, A., & Liao, W. (2023). High-efficiency carbon dioxide capture using an algal amino acid salt solution. *Journal of CO2 Utilization*, *69*, 102394. https://doi.org/https://doi-org.proxy2.cl.msu.edu/10.1016/j.jcou.2023.102394

Solomon, S., Plattner, G.-K., Knutti, R., & Friedlingstein, P. (2009). Irreversible climate change due to carbon dioxide emissions. *Proceedings of the national academy of sciences*, *106*(6), 1704-1709. https://doi.org/https://doi.org/10.1073/pnas.0812721106

Song, C., Liu, Q., Qi, Y., Chen, G., Song, Y., Kansha, Y., & Kitamura, Y. (2019). Absorption-microalgae hybrid CO2 capture and biotransformation strategy—a review. *International Journal of Greenhouse Gas Control*, *88*, 109-117. https://doi.org/https://doi.org/10.1016/j.ijggc.2019.06.002

Song, H.-J., Park, S., Kim, H., Gaur, A., Park, J.-W., & Lee, S.-J. (2012). Carbon dioxide absorption characteristics of aqueous amino acid salt solutions. *International Journal of Greenhouse Gas Control*, *11*, 64-72. https://doi.org/10.1016/j.ijggc.2012.07.019

Stetten, M. R., & Katzen, H. M. (1961). Degradation of glycogen by alkali. *Journal of the American Chemical Society*, *83*(13), 2912-2918.

Sun, B., Wang, Z., He, Q., Fan, W., & Cai, S. (2017). Porous double network gels with high toughness, high stretchability and fast solvent-absorption. *Soft matter*, *13*(38), 6852-6857. https://doi.org/https://doi.org/10.1039/C7SM01102D

Sun, J.-Y., Zhao, X., Illeperuma, W. R. K., Chaudhuri, O., Oh, K. H., Mooney, D. J.,…Suo, Z. (2012). Highly stretchable and tough hydrogels. *Nature*, *489*(7414), 133-136. https://doi.org/10.1038/nature11409

Tucker, M. (1995). Carbon dioxide emissions and global GDP. *Ecological Economics*, *15*(3), 215-223. https://doi.org/https://doi.org/10.1016/0921-8009(95)00045-3

Uludag-Demirer, S., Smerigan, A., Hsiao, P., Marks, A., Smith Iii, M. R., & Liao, W. (2023). Enhanced Carbon Dioxide Capture Using a Mixed Amino Acid Salt Solution. *Industrial & Engineering Chemistry Research*, *62*(9), 4064-4072. https://doi.org/https://pubs.acs.org/doi/10.1021/acs.iecr.2c03533

Van Tran, V., Park, D., & Lee, Y.-C. (2018). Hydrogel applications for adsorption of contaminants in water and wastewater treatment. *Environmental Science and Pollution Research*, *25*(25), 24569-24599. https://doi.org/10.1007/s11356-018-2605-y

Ying, B., & Liu, X. (2021). Skin-like hydrogel devices for wearable sensing, soft robotics and beyond. *Iscience*, *24*(11). https://doi.org/https://doi-org.proxy2.cl.msu.edu/10.1016/j.isci.2021.103174

Zahed, M. A., Movahed, E., Khodayari, A., Zanganeh, S., & Badamaki, M. (2021). Biotechnology for carbon capture and fixation: Critical review and future directions. *Journal of Environmental Management*, *293*, 112830. https://doi.org/https://doi.org/10.1016/j.jenvman.2021.112830

Zhang, L., Li, K., Xiao, W., Zheng, L., Xiao, Y., Fan, H., & Zhang, X. (2011). Preparation of

collagen–chondroitin sulfate–hyaluronic acid hybrid hydrogel scaffolds and cell compatibility in vitro. *Carbohydrate Polymers*, *84*(1), 118-125. https://doi.org/https://doi.org/10.1016/j.carbpol.2010.11.009

Zhang, Z., Li, Y., Zhang, W., Wang, J., Soltanian, M. R., & Olabi, A. G. (2018). Effectiveness of amino acid salt solutions in capturing CO2: A review. *Renewable & Sustainable Energy Reviews*, *98*, 179-188. https://doi.org/10.1016/j.rser.2018.09.019

APPENDIX

A.1 EXAMPLE CALCULATION OF CO_2 ABSORPTION CAPACITY FROM AN ABSORPTION TRIAL

When calculating final CO_2 absorption capacity after an absorption trial, the input values are reactor temperature (T), volume of airspace in the reactor (V), the initial concentration of CO_2 in the reactor (C), the initial pressure reading in the reactor (Pi), and the total pressure loss within the reactor (Pm). The volume of airspace in the reactor is calculated by subtracting the volume of absorbent material used from the 0.3 L volume of the reactor. This example calculation uses the input values from an absorption trial run at 30% CO_2 for a porous gel piece holding 20 mL of MAASS: T = 296 K, V = 0.280 L, C = 28.4%, Pi = 3.27 inH_2O, and Pm = 99.75 inH_20.

- Step 1. Add the initial pressure reading in the reactor to atmospheric pressure and convert to atm units.

$$P = 1\ atm + \left(\frac{0.00246\ atm}{inH_2O} * 3.27\ inH_2O\right) = 1.01\ atm$$

(Eq. A1)

- Step 2. Calculate initial volumes of CO_2 gas (L) and nitrogen gas (L) in the reactor using the measured initial percentage of CO_2 in the reactor.

$$V_{CO_2} = 0.280\ L * 28.4\% = 0.0795\ L$$

(Eq. A2)

$$V_{Nitrogen} = 0.280\ L - 0.0795\ L = 0.201\ L$$

(Eq. A3)

- Step 3. Convert the initial gas amounts to mol using the ideal gas equation (n = PV/RT) and the values calculated in steps 1 and 2.

$$mol_{CO_2} = \frac{1.01\ atm * 0.0795\ L}{0.0821\ \frac{L\ atm}{K\ mol} * 296\ K} = 0.00330\ mol$$

(Eq. A4)

$$mol_{Nitrogen} = \frac{1.01\ atm * 0.201\ L}{0.0821\ \frac{L\ atm}{K\ mol} * 296\ K} = 0.00832\ mol$$

(Eq. A5)

- Step 4. Calculate the total amount of gas (mol) initially present in the reactor by summing the values calculated in step 3.

$$mol_{gas} = 0.00330\ mol + 0.00832\ mol = 0.0116\ mol$$

(Eq. A6)

- Step 5. Calculate the final pressure in the reactor (atm) by subtracting the total pressure loss within the reactor (Pm) from the initial pressure calculated in step 1.

$$P = 1.01\ atm - \left(99.75\ inH_2O * \frac{0.00246\ atm}{inH_2O}\right) = 0.763\ atm$$

(Eq. A7)

- Step 6. Calculate the final moles of gas in the reactor using the ideal gas equation (n = PV/RT) and the final pressure calculated in step 5.

$$mol_{gas} = \frac{0.763\ atm * 0.280\ L}{0.0821\ \frac{L\ atm}{K\ mol} * 296\ K} = 0.00880\ mol$$

(Eq. A8)

- Step 7. Calculate the final volume of CO_2 gas in the reactor (L) using the ideal gas equation (V = nRT/P), the initial moles of nitrogen calculated in step 3, and the values calculated in steps 5 and 6.

$$mol_{CO_2\ in\ reactor} = 0.00880\ mol - 0.00832\ mol = 0.000476\ mol$$

(Eq. A9)

- Step 8. Calculate the mass of CO_2 absorbed (g) using the initial moles of CO_2 in the reactor (calculated in step 3), the final moles of CO_2 in the reactor (calculated in step 7),

and the molar mass of CO_2 (44.01 g/mol).

$$mol_{CO_2\ absorbed} = 0.00330\ mol - 0.000476\ mol = 0.00283\ mol$$

(Eq. A10)

$$mass_{CO_2\ absorbed} = 0.00283\ mol * 44.01 \frac{g}{mol} = 0.124\ g$$

(Eq. A11)

- Step 9. Calculate the volume of CO_2 absorbed (mL) using the ideal gas equation (V = nRT/P) and the values calculated in steps 5 and 8.

$$V_{CO_2\ absorbed} = \frac{0.00283\ mol * 0.0821\ \frac{L\ atm}{K\ mol} * 296\ K}{0.763\ atm} * \frac{1000\ mL}{L} = 89.9\ mL$$

(Eq. A12)

A.2 R-GENERATED PLOTS FOR AMINO ACID LEVELS IN THE GEL VS. IN THE CONTROL

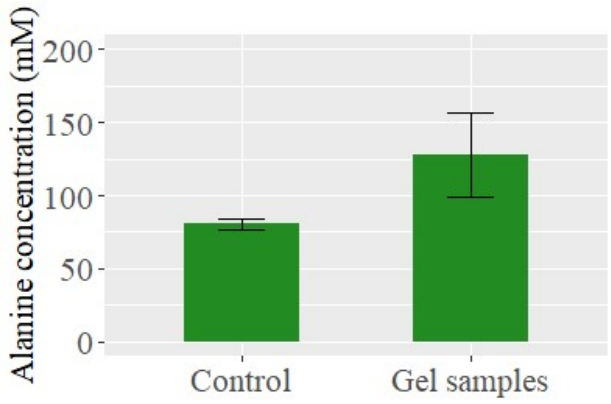

Figure A 1. Alanine concentration in the gel vs. in the control liquid.

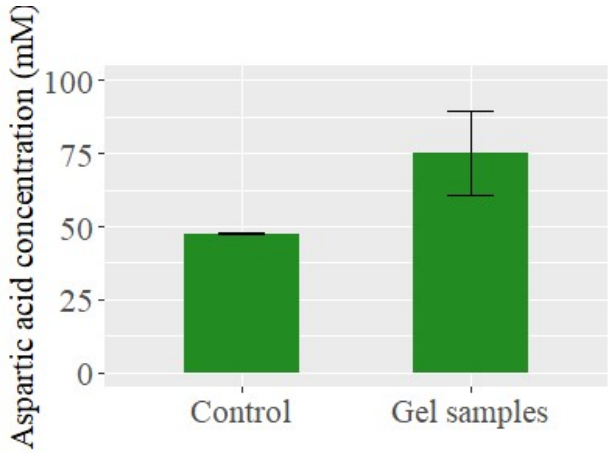

Figure A 2. Aspartic acid concentration in the gel vs. in the control liquid.

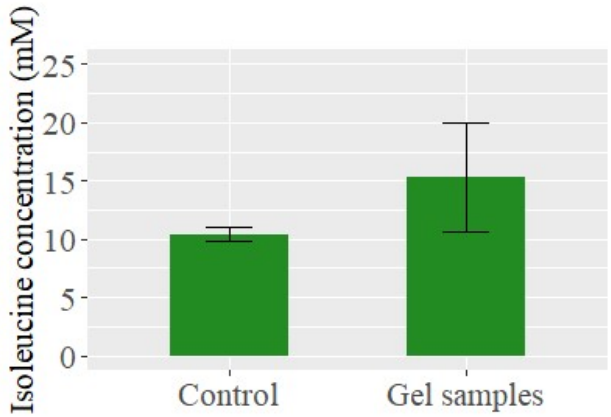

Figure A 3. Isoleucine concentration in the gel vs. in the control liquid.

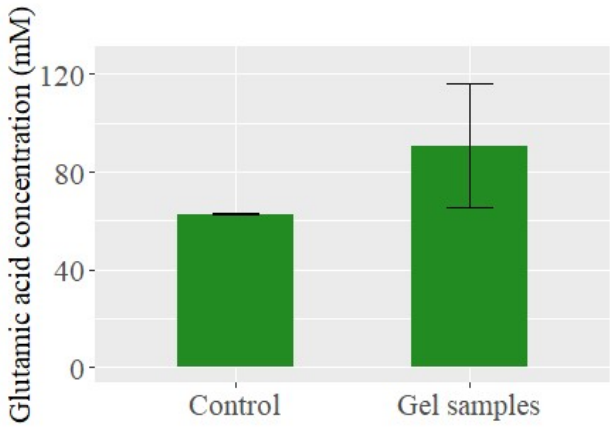

Figure A 4. Glutamic acid concentration in the gel vs. in the control liquid.

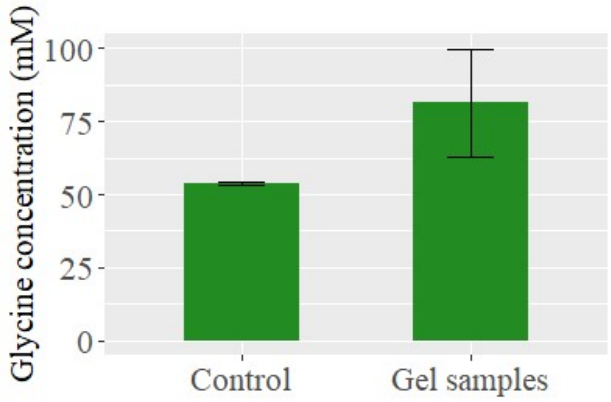

Figure A 5. Glycine concentration in the gel vs. in the control liquid.

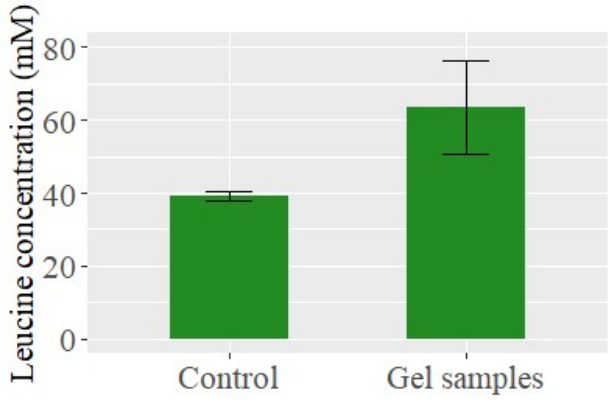

Figure A 6. Leucine concentration in the gel vs. in the control liquid.

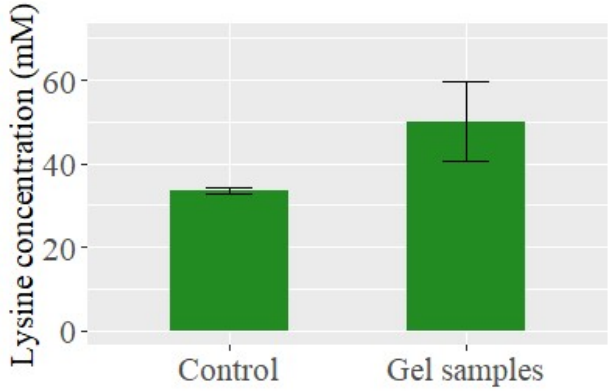

Figure A 7. Lysine concentration in the gel vs. in the control liquid.

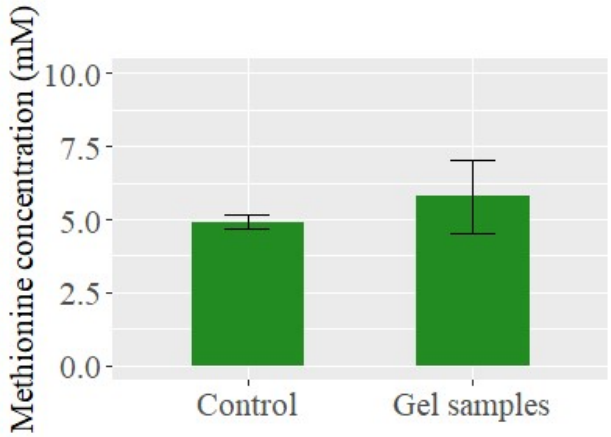

Figure A 8. Methionine concentration in the gel vs. in the control liquid.

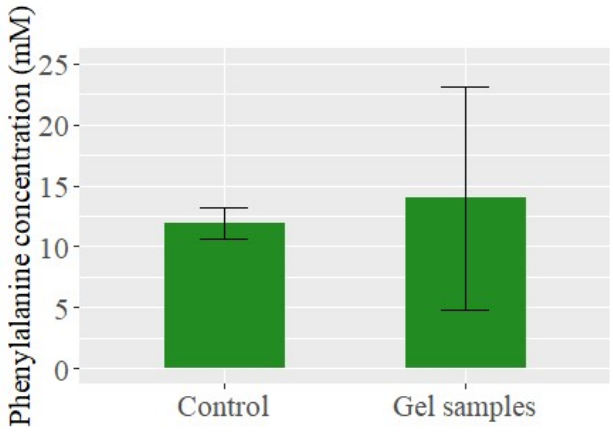

Figure A 9. Phenylalanine concentration in the gel vs. in the control liquid.

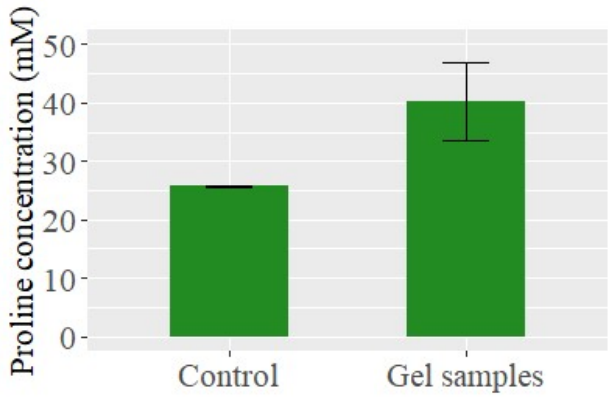

Figure A 10. Proline concentration in the gel vs. in the control liquid.

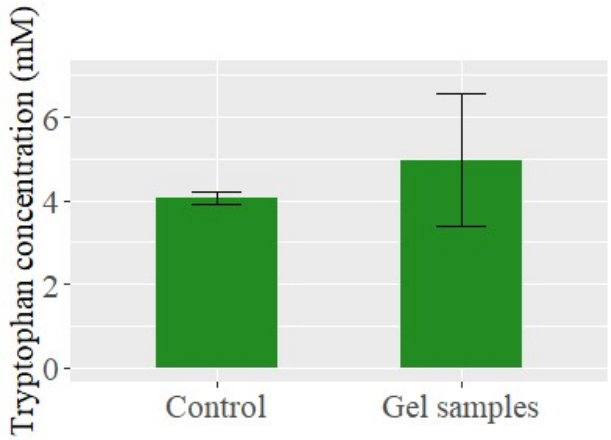

Figure A 11. Tryptophan concentration in the gel vs. in the control liquid.

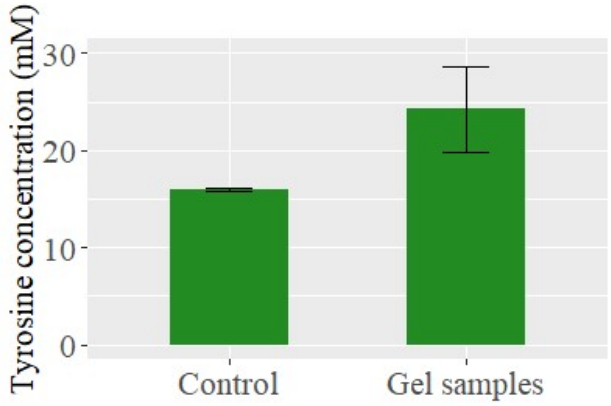

Figure A 12. Tyrosine concentration in the gel vs. in the control liquid.

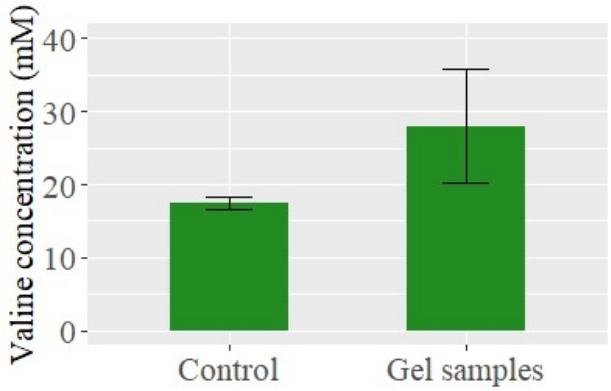

Figure A 13. Valine concentration in the gel vs. in the control liquid.

A.3 R-GENERATED PLOTS COMPARING AMINO ACID LEVELS IN THE GEL AT DIFFERENT GEL SIZES

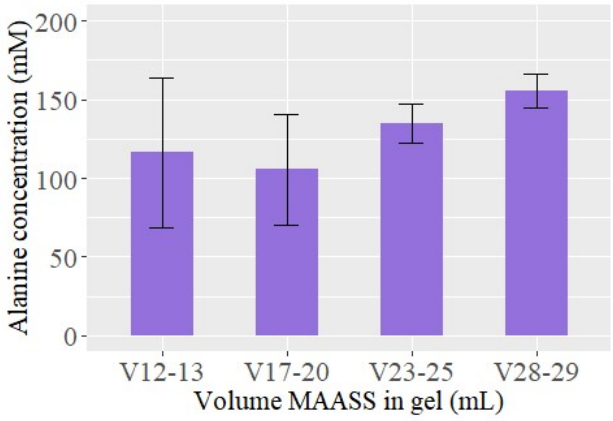

Figure A 14. Alanine concentration in the gel at different gel sizes.

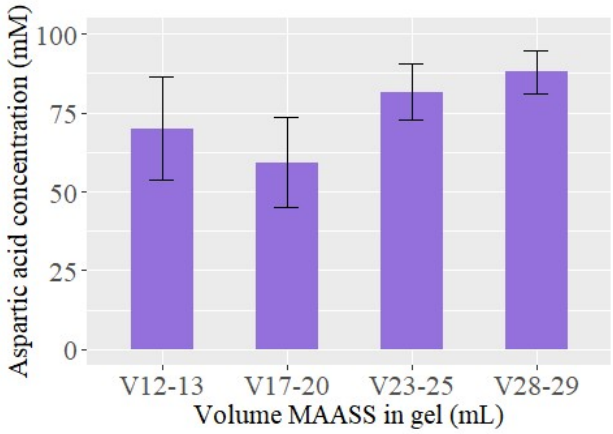

Figure A 15. Aspartic acid concentration in the gel at different gel sizes.

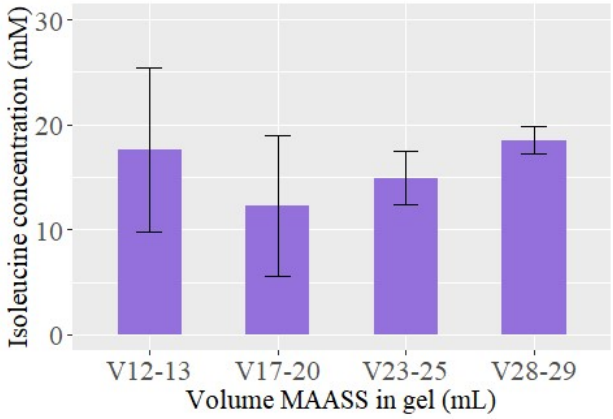

Figure A 16. Isoleucine concentration in the gel at different gel sizes.

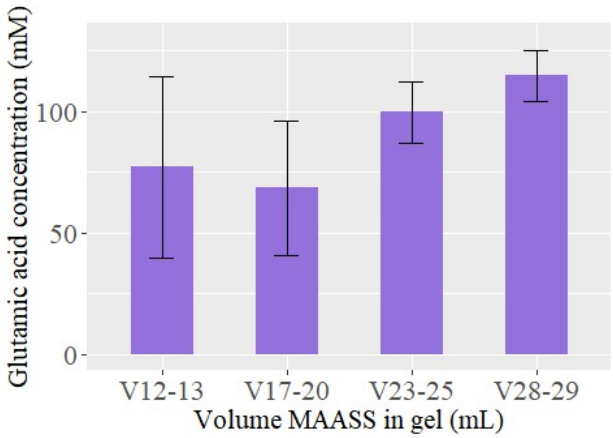

Figure A 17. Glutamic acid concentration in the gel at different gel sizes.

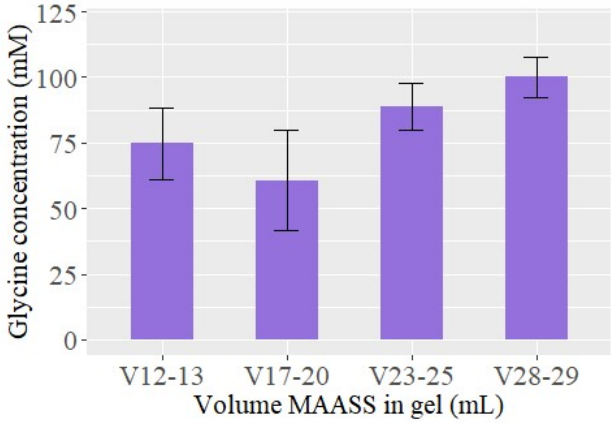

Figure A 18. Glycine concentration in the gel at different gel sizes.

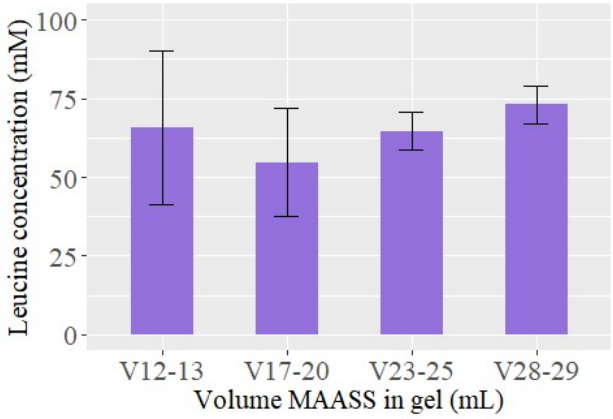

Figure A 19. Leucine concentration in the gel at different gel sizes.

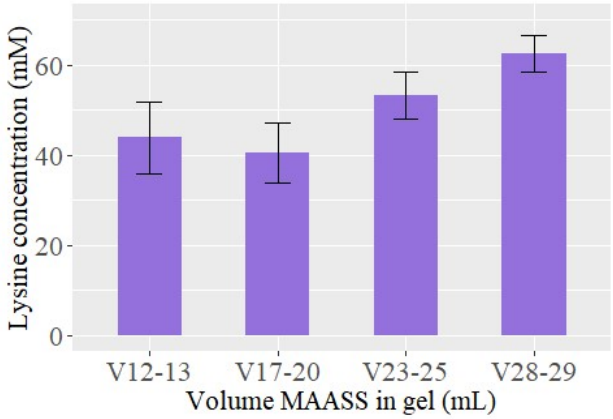

Figure A 20. Lysine concentration in the gel at different gel sizes.

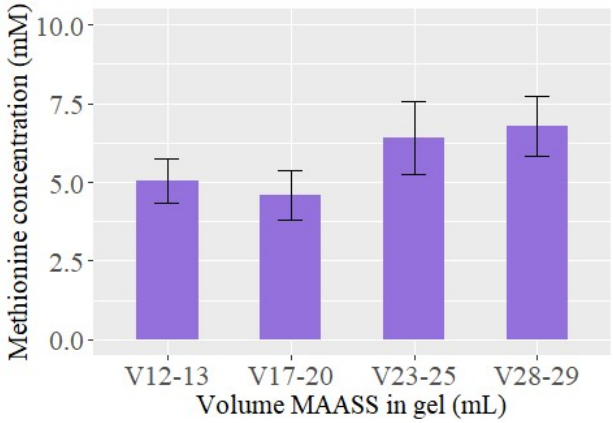

Figure A 21. Methionine concentration in the gel at different gel sizes.

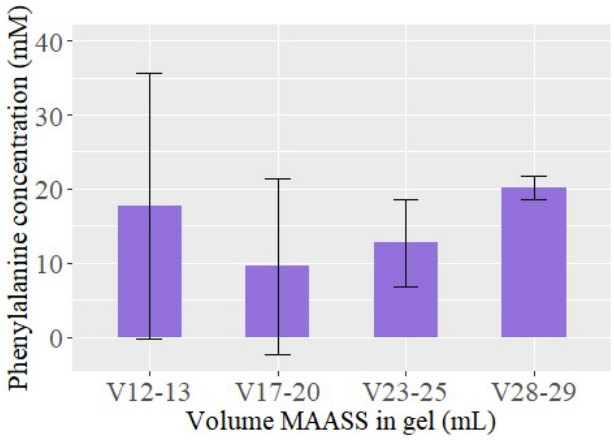

Figure A 22. Phenylalanine concentration in the gel at different gel sizes.

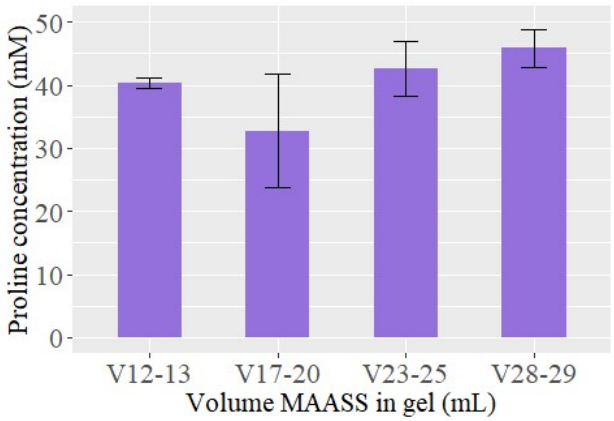

Figure A 23. Proline concentration in the gel at different gel sizes.

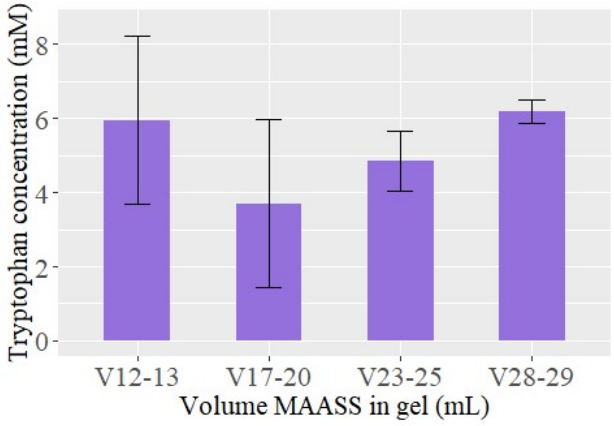

Figure A 24. Tryptophan concentration in the gel at different gel sizes.

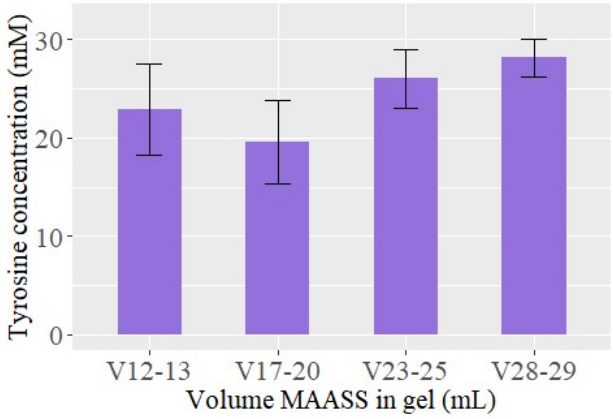

Figure A 25. Tyrosine concentration in the gel at different gel sizes.

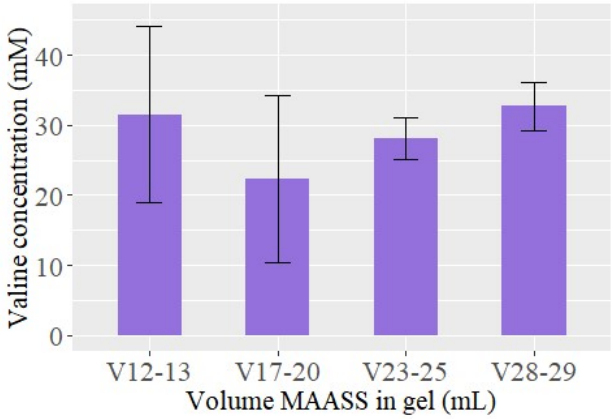

Figure A 26. Valine concentration in the gel at different gel sizes.

A.4 SUPPORTING FIGURES FROM R STATISTICAL ANALYSIS ON CO_2 ABSORPTION

A.4.1 Figures for 10% CO_2 concentration

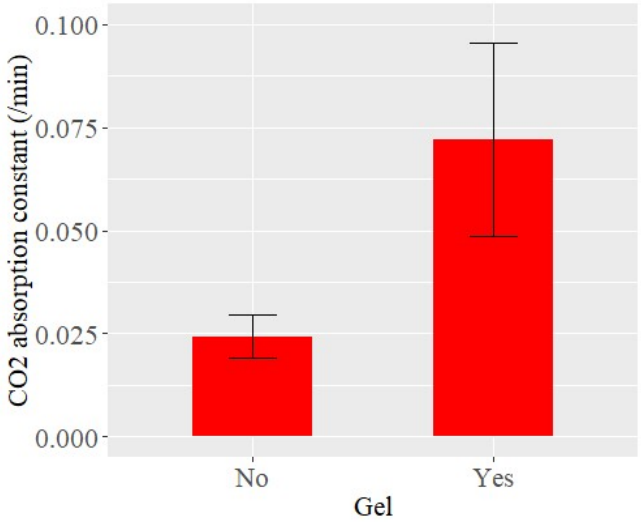

Figure A 27. Comparison of CO_2 absorption constants at 10% CO_2 concentration for with and without porous gel.

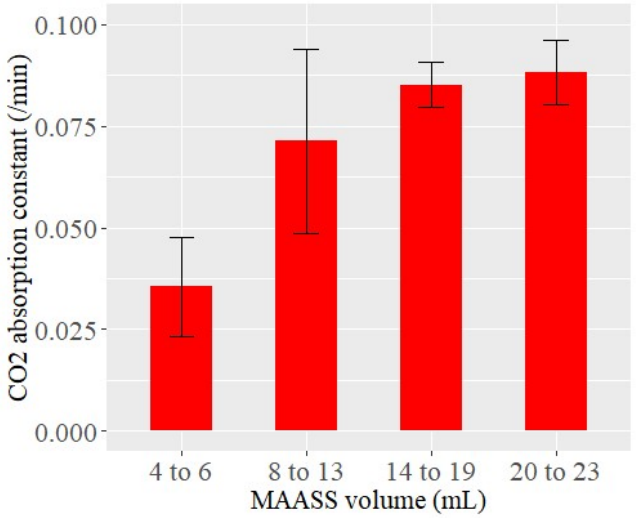

Figure A 28. Comparison of CO_2 absorption constants at 10% CO_2 concentration across MAASS volumetric categories.

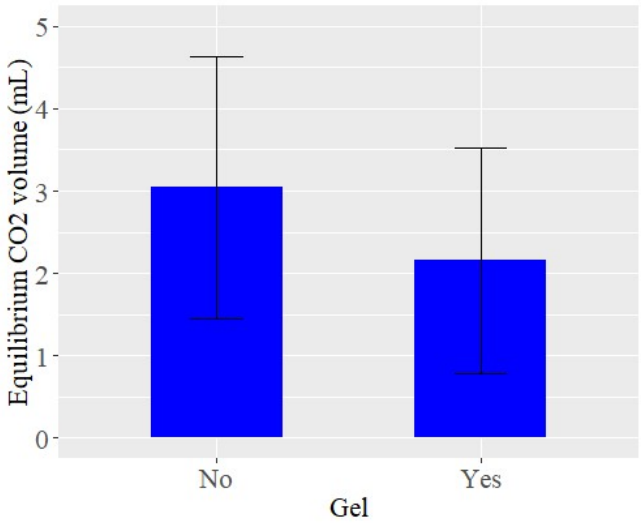

Figure A 29. Comparison of CO_2 equilibrium absorption volume at 10% CO_2 concentration for with and without porous gel.

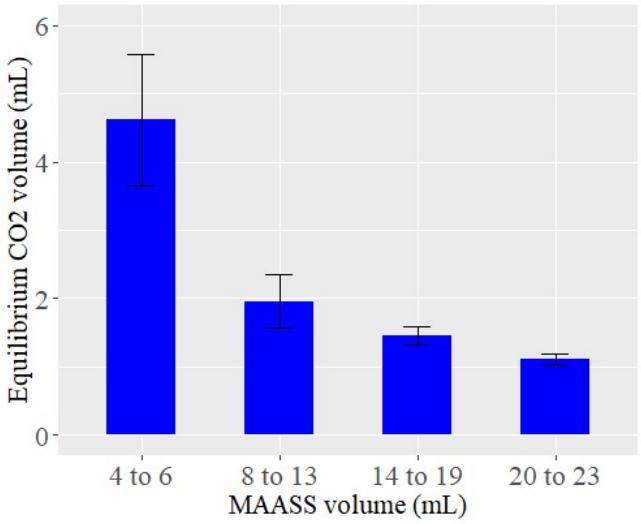

Figure A 30. Comparison of CO_2 equilibrium absorption volume at 10% CO_2 concentration across volumetric categories.

A.4.2 Figures for 30% CO_2 concentration

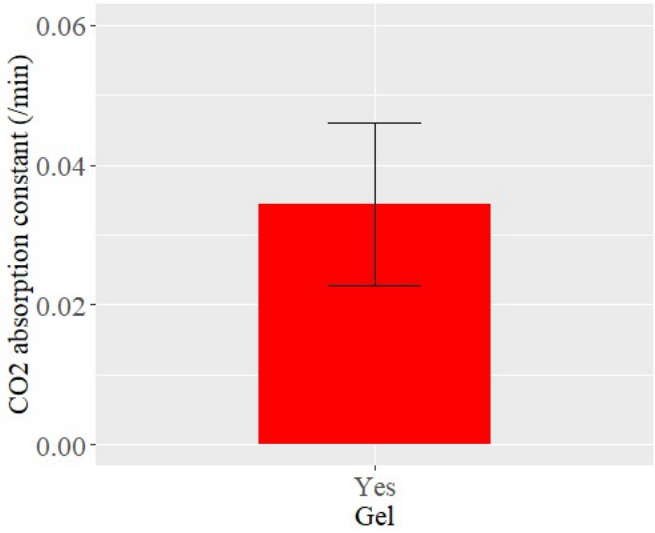

Figure A 31. Average CO_2 absorption constant for 30% CO_2 concentration porous gel trials.

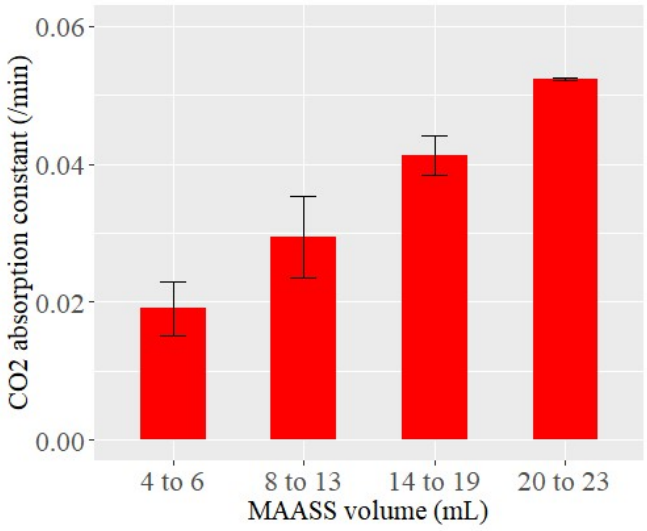

Figure A 32. Comparison of CO_2 absorption constants at 30% CO_2 concentration across MAASS volumetric categories.

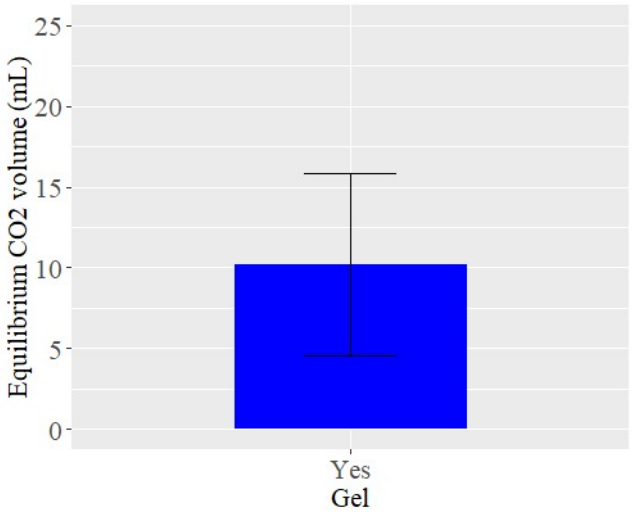

Figure A 33. Average CO_2 equilibrium absorption volume for 30% CO_2 concentration porous gel trials.

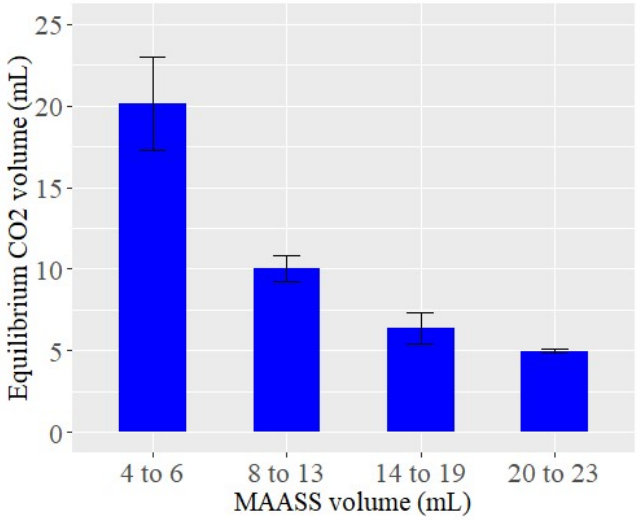

Figure A 34. Comparison of equilibrium CO_2 absorption volume at 30% CO_2 concentration across MAASS volumetric categories.

A.4.3 Figures for 50% CO_2 concentration

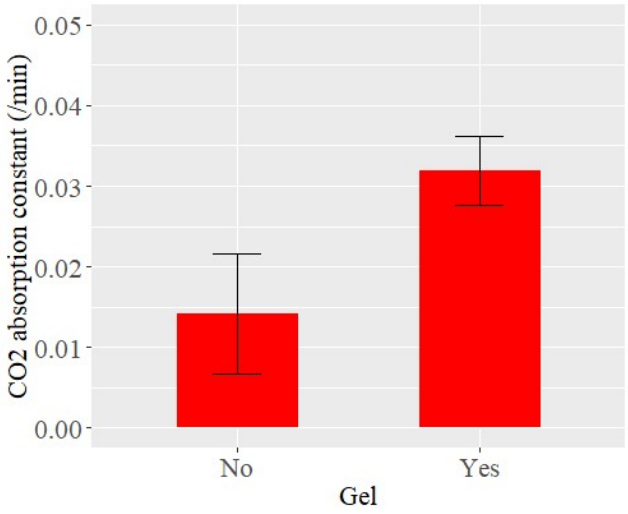

Figure A 35. Comparison of CO_2 absorption constants at 50% CO_2 concentration for with and without porous gel.

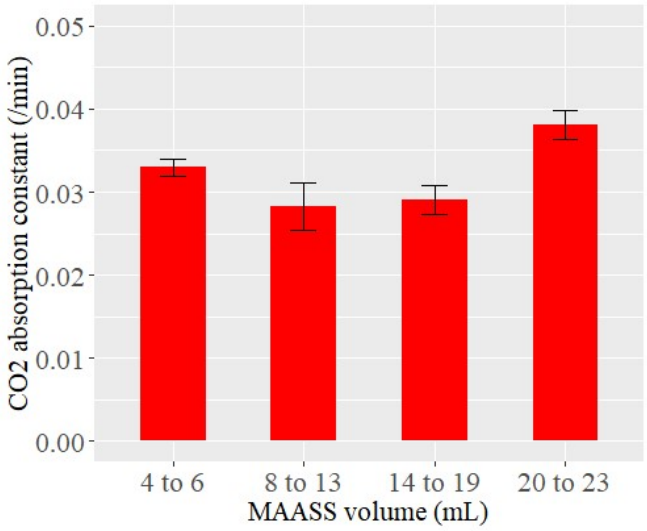

Figure A 36. Comparison of CO_2 absorption constants at 50% CO_2 concentration across MAASS volumetric categories.

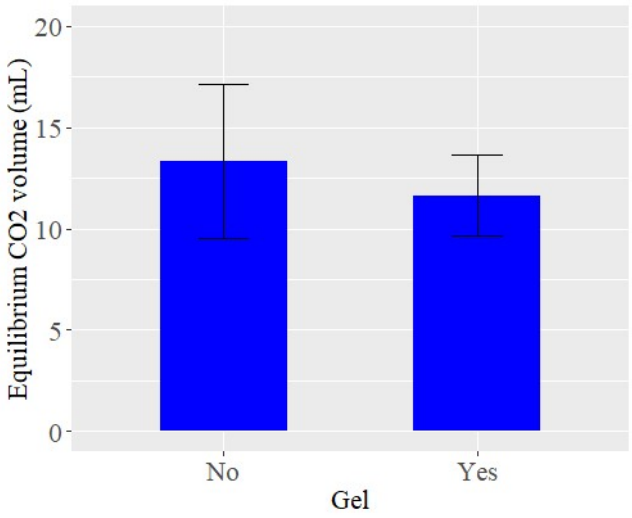

Figure A 37. Comparison of CO_2 equilibrium absorption volume at 50% CO_2 concentration for with and without porous gel.

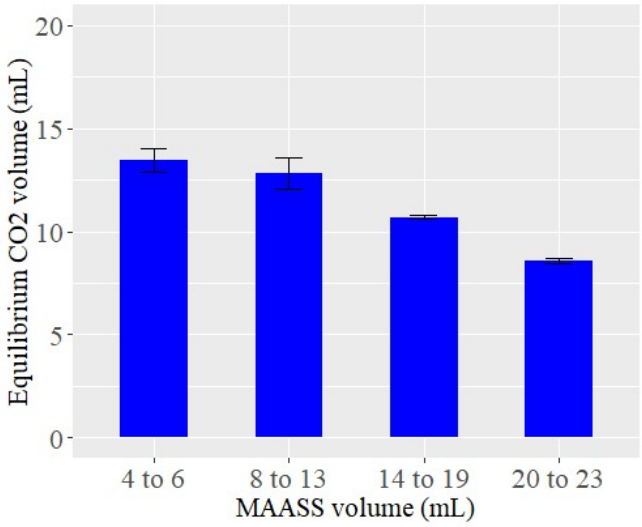

Figure A 38. Comparison of equilibrium CO_2 absorption volume at 50% CO_2 concentration across MAASS volumetric categories.

A.5 R-CODE USED FOR ANOVA AND TUKEY PAIR-WISE COMPARISON

STATISTICAL TESTS ON CO_2 ABSORPTION DATA

```
## LOADING LIBRARIES -------------------------------------------------------

library(MASS)
library(ggplot2)
library(grid)
library(gridExtra)
library(ggpubr)
library(plyr)
library(extrafont)

# FUNCTION TO CALCULATE THE MEAN AND THE STANDARD DEVIATION
# FOR EACH GROUP ----------------------------------------------------------------
# data : a data frame
# varname : the name of a column containing the variable
#to be summarized
# groupnames : vector of column names to be used as
# grouping variables
data_summary <- function(data, varname, groupnames){
  require(plyr)
  summary_func <- function(x, col){
    c(mean = mean(x[[col]], na.rm=TRUE),
      sd = sd(x[[col]], na.rm=TRUE))
  }
  data_sum<-ddply(data, groupnames, .fun=summary_func,
                  varname)
  data_sum <- rename(data_sum, c("mean" = varname))
  return(data_sum)
}


## DATA INPUT--------------------------------------------------------------

#data input by csv file
metadata <-read.csv("MetaData10.csv")
head(metadata)
View(metadata)

# Defining factors

metadata$Gel <- factor(metadata$Gel) ##Factor Statement
metadata$MAASS_Vol <- factor(metadata$MAASS_Vol) ##Factor Statement
```

```
## TWO-WAY ANOVA ON ALL DATA----------------------------------------------------

# On CO2 absorption constant

fit1 <- aov(Absorption_constant~Gel*MAASS_Vol, data = metadata)
summary(fit1) # P-value
# TUKEY MULTIPLE COMPARISON -----
Tukey1 <- TukeyHSD(fit1, conf.level=0.95) #Tukey multiple comparison
Tukey1

# On CO2 equilibrium volume

fit2 <- aov(E_Vol~Gel*MAASS_Vol, data = metadata)
summary(fit2) # P-value
# TUKEY MULTIPLE COMPARISON -----
Tukey2 <- TukeyHSD(fit2, conf.level=0.95) #Tukey multiple comparison
Tukey2


## STATISTICS ON THE DATA WITHOUT GEL ------------------------------------------

#Data selection
data1<-metadata[which(metadata$Gel=="No"),] # select the data without gel
data1

# Define the factor
data1$MAASS_Vol <- factor(data1$MAASS_Vol) ##Factor Statement


## One-way anova on grouped data-----------------------------

# Absorption constant
fit3 <- aov(Absorption_constant~MAASS_Vol, data = data1)
summary(fit3) # P-value
## TUKEY MULTIPLE COMPARISON -----
Tukey3 <- TukeyHSD(fit3, conf.level=0.95) #Tukey multiple comparison
Tukey3

# Equilibrium volume
fit4 <- aov(E_Vol~MAASS_Vol, data = data1)
summary(fit4) # P-value
## TUKEY MULTIPLE COMPARISON -----
Tukey4 <- TukeyHSD(fit4, conf.level=0.95) #Tukey multiple comparison
Tukey4

## STATISTICS ON THE DATA WITH GEL ---------------------------------------------
```

```
#Data selection
data2<-metadata[which(metadata$Gel=="Yes"),] # select the data without gel

# Define the factor
data2$MAASS_Vol <- factor(data2$MAASS_Vol) ##Factor Statement

# One-way anova

# Absorption constant
fit5 <- aov(Absorption_constant~MAASS_Vol, data = data2)
summary(fit5) # P-value
## TUKEY MULTIPLE COMPARISON -----
Tukey5 <- TukeyHSD(fit5, conf.level=0.95) #Tukey multiple comparison
Tukey5

# Equilibrium volume
fit6 <- aov(E_Vol~MAASS_Vol, data = data2)
summary(fit6) # P-value
## TUKEY MULTIPLE COMPARISON -----
Tukey6 <- TukeyHSD(fit6, conf.level=0.95) #Tukey multiple comparison
Tukey6
```

A.6 R-CODE USED FOR 3D PARETO ANALYSIS OF ABSORPTION DATA

```
# Loading the libraries
library(rgl)
library(mco)
#library(rPref)
library(dplyr)
#library(igraph)
#library(ggplot2)
#library(rmoo)

library(extrafont)
font_import() ##It needs to run individually, and may take a few minutes to import.
loadfonts(device="win")

# Load your dataset "3D-CO2-MOO-meta_data(10-percent).csv"

## Data input by csv file
data <- read.csv('3D-CO2-MOO-meta_data(10-percent).csv')
data
# Function to calculate the mean and the standard deviation for each group -----
# data : a data frame
```

```
# varname : the name of a column containing the variable
#to be summarized
# groupnames : vector of column names to be used as
# grouping variables
data_summary <- function(data, varname, groupnames){
  require(plyr)
  summary_func <- function(x, col){
    c(mean = mean(x[[col]], na.rm=TRUE),
      sd = sd(x[[col]], na.rm=TRUE))
  }
  data_sum<-ddply(data, groupnames, .fun=summary_func,
                  varname)
  data_sum <- rename(data_sum, c("mean" = varname))
  return(data_sum)
}

## the Pareto front ------------------------------------------------------
# Function to determine if a point is dominated
is_dominated <- function(row, data) {
  any(apply(data, 1, function(other) all(other <= row) & any(other < row)))
}

# Identify the Pareto front
pareto_front <- data %>%
  filter(!apply(data, 1, function(row) is_dominated(row, data)))

print(pareto_front)

# Plot the 3D Pareto front
plot3d(
  pareto_front$Absorption_constant, pareto_front$E_Vol, pareto_front$MAASS_Vol,
  col = "blue", size = 2, type = "s",
  xlab = "CO2 absorption constant (/min)", ylab = "CO2 equilibrium volume (mL CO2/mL
MAASS)", zlab = "MAASS volume in gel (mL)"
)

# Add labels (row names) to the points in the 3D plot
text3d(
  pareto_front$Absorption_constant,pareto_front$E_Vol,pareto_front$MAASS_Vol,
  texts = row.names(pareto_front),
  col = "black", cex = 0.8, adj = 2.0
)


## Generate 3D non-linear regression model using an exponential function z =
d+a*exp(b1*x+b2*y)--------------------------------
```

```
fit <- nls(pareto_front$MAASS_Vol ~ d+a*exp(b*pareto_front$Absorption_constant +
c*pareto_front$E_Vol),
        data=pareto_front, start=list(a=100, b=-1, c=-1, d=-1))
summary(fit)


# Create a grid of x and y values for the 3D non-linear regression line

# Calculate E_Vol_mean
CO2_E_Vol <- data_summary(data, varname="E_Vol", groupnames=c("MAASS_Vol"))
CO2_E_Vol$MAASS_Vol=as.factor(CO2_E_Vol$MAASS_Vol)
E_vol_mean <- CO2_E_Vol$E_Vol
E_vol_mean

# Calculate CO2_absorption_constant_mean
CO2_Absorption_constant <- data_summary(data, varname="Absorption_constant",
groupnames=c("MAASS_Vol"))
CO2_Absorption_constant$MAASS_Vol=as.factor(CO2_Absorption_constant$MAASS_Vol)
Absorption_constant_mean <- CO2_Absorption_constant$Absorption_constant
Absorption_constant_mean

# Use the fitted model to calculate MAASS_Vol
# Create the newdata with Absorption_constant_mean and E_Vol_mean and MAASS_Vol_pred
newdata = data.frame(x=Absorption_constant_mean, y=E_vol_mean,
MAASS_Vol_pred=3.760+373.907*exp(-16.442*Absorption_constant_mean-
1.594*E_vol_mean)
)
newdata

# Add the regression line to the plot
lines3d(newdata$x, newdata$y,  newdata$MAASS_Vol_pred, col = "red", lwd=3)
```

A.7 R-CODE USED FOR NSGA ANALYSIS OF ABSORPTION DATA

```
# Loading the libraries
library(rgl)
library(mco)
#library(rPref)
library(dplyr)
#library(igraph)
#library(ggplot2)
#library(rmoo)

library(extrafont)
font_import() ##It needs to run individually, and may take a few minutes to import.
```

```
loadfonts(device="win")

# Load your dataset "3D-CO2- NSGA-meta_data_ave(all).csv"

## Data input by csv file
data <- read.csv("3D-CO2-NSGA-meta_data_ave(all).csv")


## Multi-objective function

objective_function <- function(indices) {
  # Convert indices to integers
  indices <- round(indices)  # Convert floating-point indices to nearest integer

  # Ensure indices are within valid bounds (1 to n_processes)
  indices <- pmin(pmax(indices, 1), n_processes)

  selected_data <- data[indices, ]

  # Objective 1: Maximize E_Vol (mean of selected processes)
  E_Vol_max <- -mean(selected_data$E_Vol)

  # Objective 2: Maximize Absorption_constant (maximize quality by minimizing negative)
  Absorption_constant_max <- -mean(selected_data$Absorption_constant)

  # Objective 3: Minimize MAASS_Vol
  MAASS_Vol_min <- mean(selected_data$MAASS_Vol)

  return(c(E_Vol_max, Absorption_constant_max, MAASS_Vol_min))
}

# Set the parameters for optimization
dimension <- 11       # Number of process options to be selected (11 rows from the dataset)
n_processes <- nrow(data)

# Define lower and upper bounds correctly
lower_bounds <- rep(1, dimension)             # Define lower bounds as a numeric vector
upper_bounds <- rep(n_processes, dimension)   # Define upper bounds as a numeric vector

# Ensure bounds are of correct type (numeric vectors)
lower_bounds <- as.numeric(lower_bounds)
upper_bounds <- as.numeric(upper_bounds)


# Run NSGA-II (allowing replicates)
result <- nsga2(
```

```
  fn = objective_function,     # Objective function for optimization
  idim = dimension,            # Number of decision variables
  odim = 3,                    # Number of objectives
  lower.bounds = lower_bounds, # Corrected lower bounds
  upper.bounds = upper_bounds, # Corrected upper bounds
  popsize = 12,                # Population size
  generations = 100            # Number of generations
)


# Access the Pareto front values
pareto_front <- result$value

# Plot the Pareto front in 3D
library(rgl)
plot3d(-pareto_front[, 1], -pareto_front[, 2], pareto_front[, 3],
       col = "blue", size = 0.5, type = "s",
       xlab = "Total E_Vol (Maximized)",
       ylab = "Absorption_constant (Maximized)",
       zlab = " MAASS_Vol (Minimized)",
       main = "3D Pareto Front")


# Add IDs (indices) to the plot
for (i in 1:nrow(pareto_front)) {
  # Get the coordinates of the point in the 3D plot
  x_coord <- -pareto_front[i, 1]
  y_coord <- -pareto_front[i, 2]  # Flipping to represent maximization
  z_coord <- pareto_front[i, 3]

  # Label each point with its corresponding index number
  text3d(x = x_coord, y = y_coord, z = z_coord,
         texts = paste0("P", i),  # Labeling each point uniquely
         cex = 1, col = "red")
}

## Data interpretation ----------------------------------------------------

# Get decision variable values for each Pareto-optimal solution
pareto_solutions <- result$par

## Creating a comparison table for different solutions
# Extract values for a few Pareto-optimal solutions
for (i in 1:12) {
  selected_indices <- pareto_solutions[i, ]
  selected_processes <- data[selected_indices, ]
```

```
  cat("Solution ", i, ":\n")
  print(selected_processes)
  cat("\nObjectives:\n")
  cat("E_Vol: ", -pareto_front[i, 1], "\n")
  cat("Absorption_constant: ", -pareto_front[i, 2], "\n")
  cat("MAASS_Vol: ", pareto_front[i, 3], "\n\n")
}
```

A.8 MATLAB CODE FOR CALCULATING COLUMN CO_2 ABSORPTION

```
%% Load the data
clear
clc
DATA = xlsread('ColumnAbs1.xlsx');
timeC = DATA(:,1);
concC = DATA(:,2);
timeA = DATA(:,3);
concA = DATA(:,4);

%% Control absorption curve fit: 'Control Curve Fit to Concentration Data'
[xDataC, yDataC] = prepareCurveData(timeC(:), concC(:));

% Set up fittype and options.
ftC = fittype('linearinterp');

% Fit model to data.
[fitresult, gof] = fit(xDataC, yDataC, ftC);

%% Column absorption curve fit: 'Abs Curve Fit to Concentration Data'
[xDataA, yDataA] = prepareCurveData(timeA(:), concA(:));

% Set up fittype and options.
ftA = fittype('linearinterp');

% Fit model to data.
[fitresultA, gofA] = fit(xDataA, yDataA, ftA);

%% Plot fits with data.
figure
hold on
h = plot(fitresult, xDataC, yDataC);
legend(h, 'CO2 conc vs. time', 'Control Curve Fit to Concentration Data', 'Location', 'SouthEast');

hA = plot(fitresultA, xDataA, yDataA);
legend(hA, 'CO2 conc vs. time', 'Abs1 Curve Fit to Concentration Data', 'Location', 'SouthEast');
```

```
% Label axes
xlabel 'time (min)'
ylabel 'CO2 conc (%)'
grid on
hold off


%% Integrate Fit
fit1 = fit(xDataA,yDataA,ftA);
endpoint = yDataA(end);
int1 = integrate(fit1,xDataA,0);

% subtract from upper limit (control column)
fitC = fit(xDataC,yDataC,ftC);
endpointC = yDataC(end);
int2 = integrate(fitC,xDataC,0);

% figure
% plot(xDataC,int2,xDataA1,int1)

abs = int2(end) - int1(end); %(%CO2*min)

%% Calculate the Ratio of moles of Carbon Dioxide Absorbed to Amino Acid
flow = (0.115*0.09)/1000; %m^3 CO2/min (for 9% CO2 in gas flow)
densityCD = 1.98; %kg/m^3
V = abs*flow; %m^3
VCO2abs = V*1000 %L
mass = abs*flow*densityCD; %kg
P = 1; %atm
R = 8.206E-5; %m^3atm/molK
T = 296; %K
moles = P*V/(R*T);

CDabsinAA = moles/0.044 %mol CD abs/L solution
```